76. Matthews JR, Wakasugi N, Virelizier JL, Yodoi J, Hay RT. Thioredoxin regulates the DNA binding activity of NF-κB by reduction of a disulphide bond involving cysteine 62. Nucleic Acids Res 1992; 20:3821–3830.

77. Yoshida S, Katoh T, Tetsuka T, Uno K, Matsui N, Okamoto T. Involvement of thioredoxin in rheumatoid arthritis: its costimulatory roles in the TNF-α-induced production of IL-6 and IL-8 from cultured synovial fibroblasts. J Immunol 1999; 163:351–358.

78. Tagaya Y, Maeda Y, Mitsui A, Kondo N, Matsui H, Hamuro J, Brown N, Arai K, Yokota T, Wakasugi H, Yodoi J. ATL-derived factor (ADF), an IL-2 receptor/Tac inducer homologous to thioredoxin; possible involvement of dithiol-reduction in the IL-2 receptor induction. EMBO J 1989; 8:757–764.

79. Toledano MB, Leonard WJ. Modulation of transcription factor NF-κB binding activity by oxidation–reduction in vitro. Proc Natl Acad Sci USA 1991; 88:4328–4332.

80. Ghosh G, van Duyne G, Ghosh S, Sigler PB. Structure of NF-κB p50 homodimer bound to a κB site. Nature 1995; 373: 303–310.

81. Muller CW, Rey FA, Sodeoka M, Verdine GL, Harrison SC. Structure of the NF-κB p50 homodimer bound to DNA. Nature 1995; 373:311–317.

82. Qin J, Clore GM, Kennedy WM, Huth JR, Gronenborn AM. Solution structure of human thioredoxin in a mixed disulfide intermediate complex with its target peptide from the transcription factor NFκB. Structure 1995; 3:289–297.

83. Sakurada S, Kato T, Okamoto T. Induction of cytokines and ICAM-1 by proinflammatory cytokines in primary rheumatoid synovial fibroblasts and inhibition by *N*-acetyl-L-cysteine and aspirin. Int Immunol 1996; 8:1483–1493.

84. Taniguchi Y, Taniguchi-Ueda Y, Mori K, Yodoi J. A novel promoter sequence is involved in the oxidative stress-induced expression of the adult T-cell leukemia-derived factor (ADF)/human thioredoxin (Trx) gene. Nucleic Acids Res 1996; 24:2746–2752.

85. Saitoh M, Nishitoh H, Fujii M, Takeda K, Tobiume K, Sawada Y, Kawabata M, Miyazono K, Ichijo H. Mammalian thiore-

Kidney International, Vol. 67 (2005), pp. 1391–1396

Positive correlation between sialyl Lewis X expression and pathologic findings in renal cell carcinoma

KEIICHI TOZAWA, TAKASHI OKAMOTO, NORIYASU KAWAI, YOSHIHIRO HASHIMOTO, YUTARO HAYASHI, and KENJIRO KOHRI

Department of Nephro-urology, Nagoya City University, Graduate School of Medical Sciences, Nagoya, Japan; and Department of Molecular Genetics, Nagoya City University, Graduate School of Medical Sciences, Nagoya, Japan

Positive correlation between sialyl Lewis X expression and pathologic findings in renal cell carcinoma.

Background. Interaction between tumor cells and endothelium plays a major role in cancer invasion and metastasis. Among various cell adhesion molecules, the cognate interaction between sialyl Lewis antigen expressed in the tumor cell surface and E-selectin expressed on endothelial cells is considered to be crucial for the tumor cell adhesion to the endothelium.

Methods. The sialyl Lewis X (sL^X) expression in 45 specimens from renal cell carcinoma patients was examined using immunohistochemistry.

Results. In this study, we demonstrate that the immunoreactivity for sL^X in renal cell carcinoma specimens not only correlates with conventional histopathologic parameters but also serves as a useful indicator for the prognosis of renal cell carcinoma.

Conclusion. Since beneficial effect of cimetidine has been reported and ascribed to its inhibitory action on the expression of E-selectin, a ligand molecule of sialyl Lewis antigen, cimetidine may also show inhibitory effect on the tumor recurrence and metastasis of renal cell carcinoma with high level of sL^X expression.

In order for tumor cells to metastasize, they first need to interact with endothelial cells. This cell-to-cell interaction requires the cognate interaction of cell adhesion molecules including E-selectin (tethering), and intercellular adhesion molecule-1 (ICAM-1) and vascular cell adhesion molecule-1 (VCAM-1) (firm adhesion) that are expressed on the endothelial cell surface. Among these cell adhesion events the tethering step and thus the interaction between E-selectin and its ligand molecule sialyl Lewis antigens is considered crucial [1]. The ligands to E-selectin are sialyl Lewis antigens include sialyl Lewis X (sL^X) and sialyl Lewis A (sL^A). Recent reports have indicated that the beneficial effects of cimetidine for the patients with colorectal cancers are ascribed to its action in inhibiting E-selectin expression on the cell surface [2, 3]. These experimental observations were confirmed by a randomized clinical trial of cimetidine, which clearly showed that the cimetidine treatment dramatically improved the survival of colorectal cancer patients with tumor cells expressing high levels of sialyl Lewis antigens but no such effects were found when sialyl Lewis expression levels were found low or null [3].

The sialyl Lewis antigen has been used as a useful marker for the diagnosis of various cancers in digestive organs, pancreas, gallbladder, liver, lung, and ovary [4–6]. The greater level of the sL^X expression was found in the metastasized lesions than the primary tumors in cases of bladder cancer [3]. Although the incidence and significance of expression of sL^X antigen in renal cell carcinoma have ever been reported by only Cordon-Cardo et al [7], cimetidine has been shown to have beneficial effects on the survival of patients with renal cell carcinoma. In addition, Kinouchi et al [8] reported that the combined therapy with interferon-α (INF-α) and cimetidine were effective even in advanced cases of renal cell carcinoma. Kobayashi et al [9] found that cimetidine could block the expression of E-selectin on the surface of human umbilical vein endothelial cells (HUVECs), which subsequently reduced the adhesion of tumor cells to the endothelium and prevented liver metastasis in a nude mice model. These findings indicate that the expression and the interaction of these cell adhesion molecules may be a rate-determining step for the initiation of the aggressive expansion of tumor cells such as invasion and metastasis.

In this study, we demonstrate that the level of cell surface expression of sL^X antigen in renal cell carcinoma tumors was correlated with the clinical outcome as well as the histopathologic characteristics. The significance of these findings is discussed in terms of the choice of adjuvant cancer therapy.

Key words: sialyl Lewis antigen, renal cell carcinoma, cimetidine.

Received for publication September 17, 2004
and in revised form November 2, 2004
Accepted for publication November 11, 2004

METHODS

Patients and samples

Forty-five patients who were diagnosed to have renal cell carcinoma and received radical nephrectomy at Nagoya City University Hospital between 1997 and 2002 were enrolled in this study. These patients were subdivided by into pT1 (14 patients), pT2 (25 patients), pT3 (five patients), and pT4 (one patient) groups according to the TNM classification of malignant tumors. Metastases were present at initial diagnosis in 11 patients (M1). No metastatic lesion was found in the other 34 patients (M0). The nuclear grading of cancer was determined based on the General Rules for Clinical and Pathological Studies on Renal Cell Carcinoma proposed by the Fuhrman's grading system. Histopathologic grading based on the nuclear morphology is as follows: grade 1, nuclei indistinguishable from those of normal tubular cells; grade 2, moderately enlarged, often irregular and slightly pleomorphic nuclei with defined nucleoli and no bizarre forms; and grade 3, numerous bizarre or giant nuclei. The classification of vascular invasion is as follows: pV0, no vascular invasion in specimen; pV1a, microscopic vascular invasion in a renal vein; pV1b, macroscopic vascular invasion in a renal vein; pV2, vascular invasion in vena cava. For the detection of distant metastasis, all the patients were checked at least twice per year for occurrence of metastasis by x-ray studies, computed tomography (CT), and bone scintigraphy during the follow-up period.

Immunohistochemistry

Paraffin-embedded tissue sections obtained from 45 patients during the operation were deparaffinized in a cleaning solution (Histochoice) (Amresco, Solon, OH, USA), rehydrated in a graded series of ethanol (100%, 95%, 70%, and 50%), and washed in distilled water. Endogenous peroxidase activity was quenched by 1.5% H_2O_2 in phosphate-buffered saline (PBS) for 15 minutes followed by washing twice with PBS. Nonspecific protein recognition by the antibody was blocked in casein wash buffer (containing 0.3% casein and 0.5% Tween-20 in PBS) for 30 minutes. Tissue sections were then incubated for 1 hour at room temperature with the primary antibody, monoclonal anti-sL^X antibody (Seikagaku Co., Tokyo, Japan), or anti-E-selectin antibody (Dako, Copenhagen, Denmark). After being washed twice in 1:10 casein wash buffer for 5 minutes, and incubated with 1:250 biotinylated antimouse IgG (Vector Laboratories, Burlingame, CA, USA) for 30 minutes, the specific intracellular immunoreactivity was detected by incubation with avidin-biotin/horseradish peroxidase complex (Vector Laboratories) for 45 minutes at room temperature followed by color development in 0.05% diaminobenzidine (DAB)/0.01% H_2O_2/PBS (pH 7.6) chromogen (Sigma Chemical Co., St. Louis, MO, USA) for 5 minutes. Color development was stopped by washing in distilled water, and sections were lightly counterstained in hematoxylin, dehydrated in a graded series of alcohol, cleared in xylene, and finally mounted in Eukitt.

Semiquantitative analysis of sL^X expression

The degree of sL^X expression was estimated and classified into one of five grades as described previously [10]. Immunoreactivity of sL^X was classified into a scale of 0 to 4 on the basis of staining of tumor cells as follows: 0, no staining; 1, focal, weak staining; 2, strong staining of <25% of cells or moderate staining of <80%; 3, strong staining of 25% to 50% or moderate staining of >80%; and 4, strong staining of >50%. The immunostained tissue section slides were examined and scored independently by two of the authors blinded to any other pathologic or clinical information. In 60% of cases the decisions were consistent, and the other 40% were reviewed until agreement was achieved.

Statistical analysis

Data are presented as the mean ± standard error of the mean (SEM). Individual groups (each pathologic grade and TNM classification) were then compared using the nonparametric Mann-Whitney U test, generalized Wilcoxon test and Student t test. For all analyses a probability value of $P < 0.05$ was considered statistically significant.

RESULTS

Among the 45 renal cell carcinoma patients enrolled in this study, 27 (60%) had grade 1 tumors, 11 (24.4%) had grade 2 tumors, and seven (15.6%) had grade 3 tumors. All the tumor tissues were examined for the expression of sL^X and compared with histopathologic findings and clinical characteristics, including the recurrence rate and the incidence of metastasis. The staining of sL^X antigen was predominantly detected in the cell membrane of tumor cells or intercellular matrix. In most cases, heterogeneity of sL^X staining was noted within individual tumor samples showing either variation in the intensity of staining or patchiness of the DAB staining (Fig. 1).

In Figure 2A, the positive correlation of semiquantitative evaluation of the sL^X expression (immunoreactivity) and the tumor staging (pT) are demonstrated. There were significant differences in sL^X expression between pT1a and pT3 ($P = 0.009$ by Mann-Whitney test), and pT2 and pT3 ($P = 0.034$). Although only single cases were assigned to pT1b and pT4, there was a strong positive correlation between the size of tumor mass and its extension and the extent of sL^X antigen expression. Interestingly, the level of sL^X expression was positively correlated

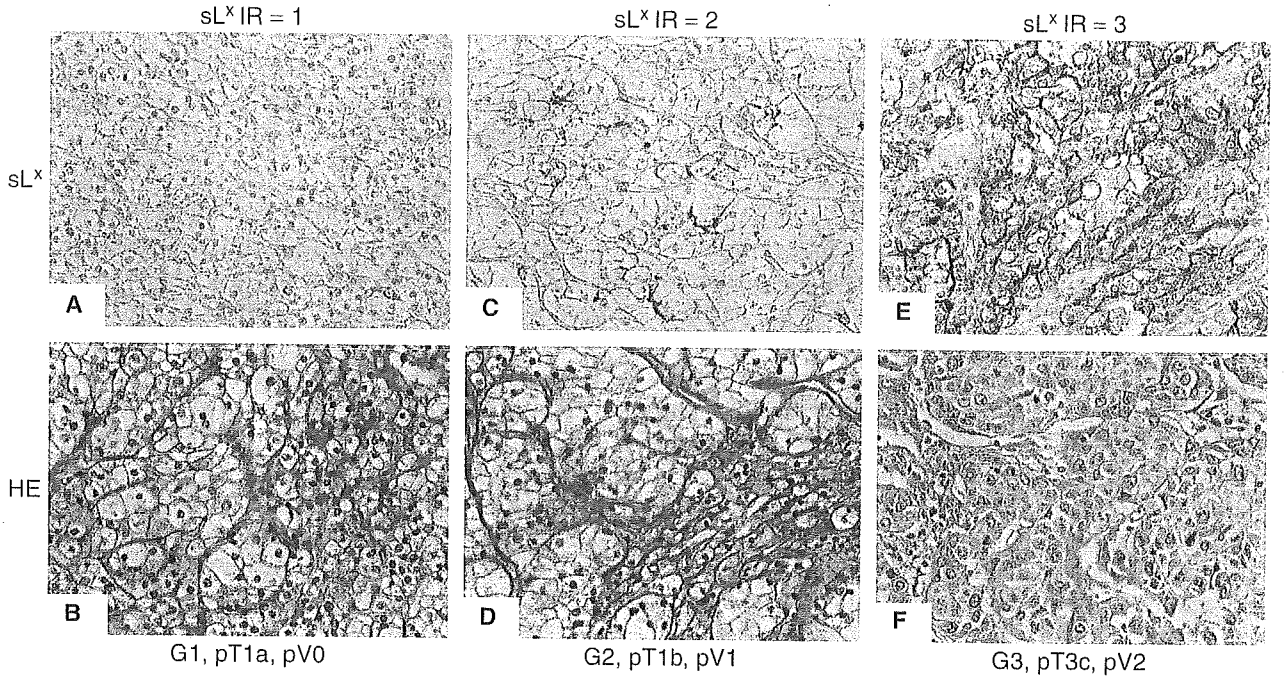

Fig. 1. Histopathologic findings of the tissue expression of sialyl Lewis X (sL^X) in renal cell carcinoma. sL^X staining of three representative renal cell carcinoma cases are presented. (*A*, C, and *E*) Immunostaining of sL^X antigen. (*B*, *D*, and *F*) Hematoxylin and eosin staining of renal cell carcinoma. The tissue sections of the same patients (A and B; C and D; and E and F) were stained. The level of sL^X expression is expressed as the immunoreactivity (IR) to the mouse monoclonal antibody to human sL^X antigen (see the **Methods** section for the details). The pathologic diagnosis, based on the General Rules for Clinical and Pathological Studies on Renal Cell Carcinoma proposed by the Japanese Urological and Pathological Association [11], of each patient is also indicated. Abbreviations are: G, nuclear morphology; pT, tumor size; pV, vascular infiltration.

with the rate of local recurrence and metastasis of cancer (collectively called "recurrence" in this study) (Fig. 2B). Among 34 patients, the tumor recurrence within 3 years after the radical nephrectomy was noted in 11 cases (32%). In these patients, the level of sL^X expression of the original tumors that were resected was significantly higher than those without recurrence.

We then looked at the extent of vascular infiltration of the original tumor tissue. Whereas no vascular infiltration of tumor cells was noted in 23 out of 24 patients without recurrence, significant vascular infiltration was evident in all the patients with tumor recurrence (11 patients). Only one patient had a sign of mild local vascular infiltration but no recurrence was detected. These findings of vascular infiltration with regard to the level of sL^X expression (immunoreactivity) are depicted in Figure 2C. These observations clearly illustrates that the tumor with high expression of sL^X antigen had a higher level of vascular infiltration ($P < 0.001$, overall). The patients with the tumor with high expression of sL^X antigen showed a significantly higher rate of tumor recurrence ($P < 0.05$). There was no significant difference between the expression of sL^X and pathologic subtypes of renal cell carcinoma.

Among 45 cases, studied 36 (80%) and nine (20%) cases were pathologically diagnosed as the clear cell type and the chromophobe cell type, respectively. However, there was no statistical significance in the level of sL^X expression with regard to the cell types. No statistical significance was found between the tumor cell type and the rate of tumor occurrence. In either cell types, the tumor of low sL^X immunoreactivity showed less probability of local recurrence. Moreover, the level of sL^X expression in patients with distant metastasis was significantly higher than that without distant metastasis ($P < 0.0001$). Thus, the expression levels of sL^X antigen appear to be a significant predictor for the development of metastases and tumor-free survival rate. In Figure 2D, we examined the relationship between the pathologic grading based on the nuclear morphology and the level of sL^X expression. Whereas most of the cases (27 patients) were classified into grade 1, tumors from 11 and seven patients were classified into grades 2 and 3, respectively. Interestingly, there was a strong difference in the levels of cell surface sL^X expression and this pathologic classification. Lower grade tumor showed significantly lower levels of sL^X expression: between grades 1 and 2 ($P = 0.04$ by Mann-Whitney test); between grades 1 and 3 ($P = 0.0002$ by Mann-Whitney test); and no statistical significance between grades 2 and 3.

Finally, we have examined the metastasis-free period by the classification based on the level of sL^X expression. As shown in Figure 3, we found a significant difference in the rate of tumor-free survival between cases with immunoreactivity ≤ 2 (low sL^X expression) and those

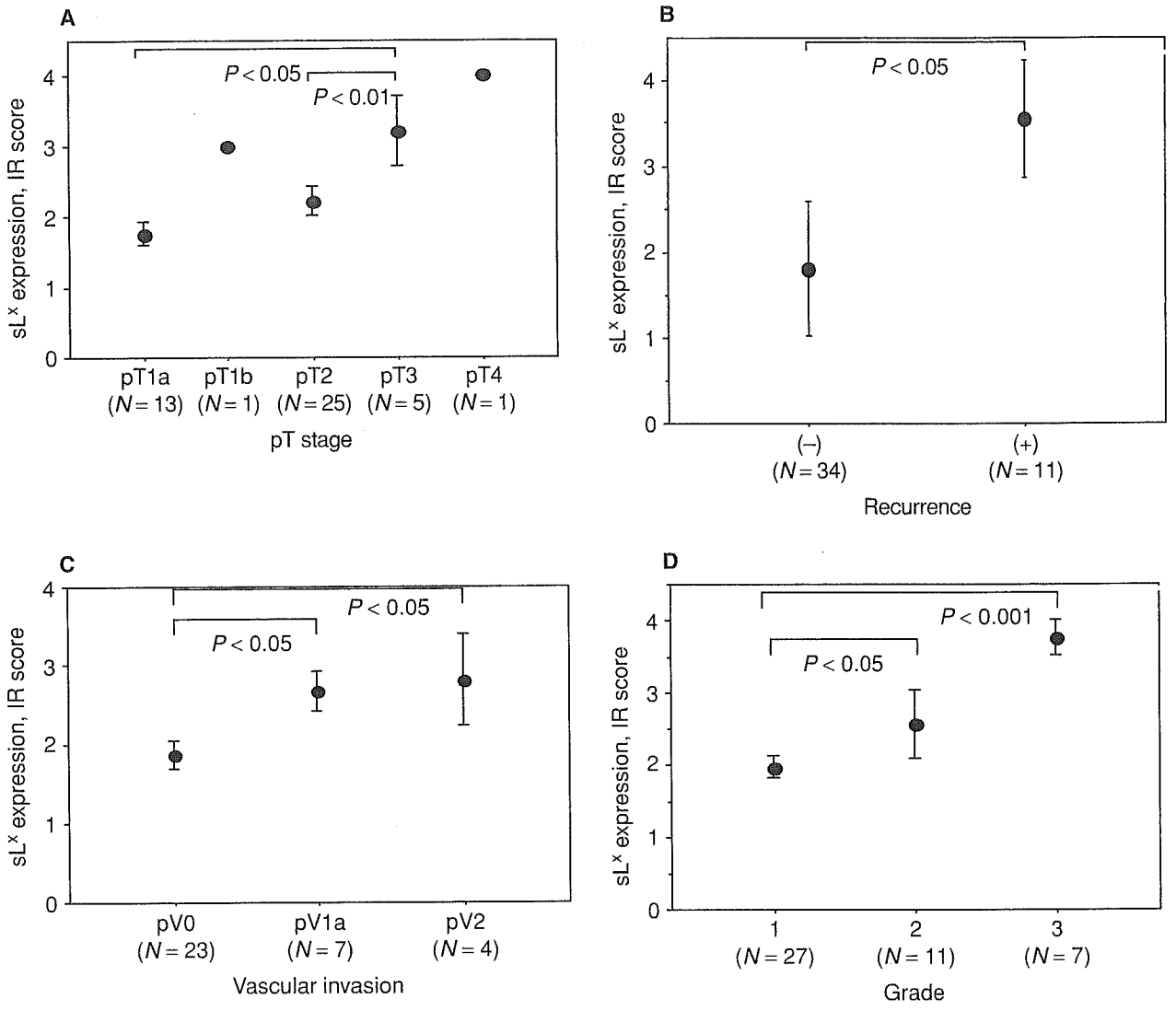

Fig. 2. Positive correlation of the level of sialyl Lewis X (sL^X) antigen expression and the tumor staging (pT), the cancer recurrence, the degree of vascular infiltration of tumor, and the nuclear grading of tumor cells. (*A*) sL^X expression of tumor tissues and T stages. The level of sL^X expression is determined according to the results of immunostaining of each tumor tissue and expressed as immunoreactivity (IR) score. The tumor tissues are classified according to the tumor staging (pT) based on the size of primary tumor. The average sL^X expression levels were compared among these groups and the differences were assessed by Mann-Whitney test. N is the number of renal cell carcinoma cases in each category. (*B*) sL^X expression and the cancer recurrence. The average sL^X expression levels were compared between groups with and without cancer recurrence (local recurrence and detection of distant metastasis). The statistical differences were found between these two groups ($P < 0.05$). (*C*) Vascular infiltration of tumor cells and sL^X expression. The extents of vascular invasion of tumor cells were determined by microscopic examination of the resected pathologic specimen obtained during surgical operation. Note that significant statistical differences ($P < 0.05$) were found between pV0 and pV1a, and pV0 and pV2. No significant differences were found between pV1a and pV2. (*D*) Positive correlation between the pathologic grading and the level of sL^X expression. The pathologic grading was determined for each case based on the nuclear morphology of tumor cells [11]. Significant differences in the level of sL^X expression were found between pathologic grades 1 and 3 ($P < 0.001$) and grades 1 and 2 ($P < 0.05$).

with immunoreactivity >2 (high sL^X expression) ($P = 0.0047$ by generalized Wilcoxon test). The cumulative 3-year tumor-free survival rate of the immunoreactivity ≤2 group of renal cell carcinoma patients ($N = 16$) was 90%, whereas that of the immunoreactivity >2 group ($N = 11$) was only 38.5%. Any greater differences were found when we classified the renal cell carcinoma cases by tumor grading, tumor cell types, or pT staging (data not shown).

DISCUSSION

Currently, urologic surgeons do not have powerful measures to assess the aggressiveness of advanced renal cell carcinoma and predict future prognosis of the patients besides pathologic diagnosis. Neither do we have any better adjuvant therapeutic options to construct effective therapeutic strategies according to the individual characteristics of tumor other than radical nephrectomy. In this study, we demonstrate that expression of sL^X

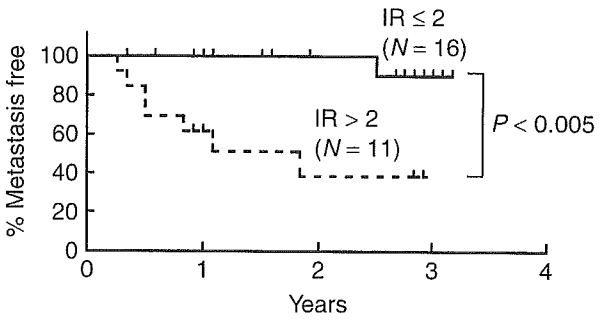

Fig. 3. The level of sialyl Lewis X (sL^X) expression and the metastasis-free period. All the renal cell carcinoma cases were classified into two groups: low sL^X expression [immunoreactivity (IR) ≤2] and high sL^X expression (IR >2). Twenty-seven cases without metastasis upon the initial diagnosis were followed up for 3 years. All patients received medical check-ups, including x-ray studies, computed tomography (CT), and whole body bone schintigraphy at least twice a year during the follow-up period. The level of sL^X expression was assessed by immunohistochemistry using the resected tumor tissue upon radical nephrectomy (year = 0). Statistically significant difference in the metastasis-free period was observed between low sL^X expression (IR ≤2) and high sL^X expression (IR >2) ($P = 0.0047$).

antigen on renal cell carcinoma tumor cells showed strong positive correlation with both macroscopic and microscopic pathologic findings, and clinical outcomes such as metastasis and tumor-free survival.

The major benefit of these findings in terms of a proposal of novel therapy comes from previous reports with colorectal cancers and the dramatic beneficial effect of cimetidine [2, 9, 11, 12]. For example, Matsumoto et al [2, 12] reported that the treatment with cimetidine markedly reduced the frequency of metastasis and significantly increased the survival rate in the patients whose tumor cells expressed higher levels of the sL^X and the sL^A epitopes. However, cimetidine was not effective in the patients with lower levels (or none) of these epitopes, although such cancers are considered to be less aggressive. It was demonstrated that a 1-year course of cimetidine produced a 10-year survival rate of 96% in patients whose tumor had high sL^X expression with cimetidine, compared to only 35% in control cases without cimetidine treatment [11]. Similar observations with cimetidine were reported with renal cell carcinoma [8].

Although the mechanism of cimetidine to endow cancer patients of high sL^X antigen expression in tumors with the beneficial effects, Kobayashi et al [9] clearly showed that this effect of cimetidine is ascribed to the down-regulation of E-selectin, a ligand molecule for sialyl Lewis antigens, that is expressed on the endothelium. They demonstrated that cimetidine could block the expression of E-selectin and thus inhibited the adhesion of tumor cells to the HUVECs and that the cimetidine administration in nude mouse model also inhibited the transsplenic liver metastasis [9]. Other possible effects of cimetidine include (*1*) inhibition of the activity of suppressor T lymphocytes bearing a histamine type 2 receptor in cancer patients [11, 13]; (*2*) cimetidine, acting as an antioxidant, inhibits tumor growth [14]; (*3*) prevention of postoperative alterations of lymphocyte subpopulations [15]; and (*4*) maintenance of natural killer cell activity [16].

Metastasis is the hallmark of malignant phenotype of cancer. The involvement of either sL^A or sL^X in adhesion to the endothelium is still controversial and may depend on the tissue types of cancers [17, 18]. The hematogenous metastasis of colorectal cancer and pancreatic cancer is mainly mediated by sL^A/E-selectin interaction [18] whereas that of renal cell carcinoma involves primarily sL^X in at least three renal cell carcinoma cell lines in cell culture experiments [19]. Furthermore, Steinbach et al [19] concluded that cytokines significantly affect the adhesion of renal cell carcinoma to the endothelium, and that cytokine-induced increases in tumor endothelial binding are mediated at least in part by the E-selectin:sL^X interaction.

In one of our previous studies [1], we reported that adhesion of tumor cell line QG90 derived from lung cancer to HUVEC was dependent on E-selectin expression on the cell surface of HUVEC. The adhesion of cancer cell to HUVEC and E-selectin expression was induced by interleukin (IL)-1β. The various inhibitors of the nuclear factor-kappaB (NF-κB) activation cascade could block the cell adhesion mediated by E-selectin and sL^X as E-selectin gene expression is under the transcriptional control of NF-κB. However, the action of cimetidine in blocking E-selectin does not appear to be at the level of transcription but rather at a step after transcription [9]. In this regard, it may be worth nothing that a possible involvement of other regulatory molecules such as p38 mitogen-activated protein kinase (MAPK), in addition to NF-κB, also participating in the IL-1β signaling [20, 21] should be examined as p38 MAPK is required for the E-selectin expression most likely at the level of post-transcription [20–25]. In this context, the issue of whether cimetidine but not other histamine receptor (H_2R) antagonists could interfere with such signaling cascade should also be explored.

The design of our study took into account the similarity between renal cell carcinoma and colorectal cancer in that cimetidine has beneficial effects on both cancers. As shown in this study, the immunoreactivity to sL^X on renal cell carcinoma specimens was remarkably correlated with T stage and tumor-free survival (Figs. 2 and 3). Semiquantitative analysis revealed that elevated expression of the sL^X epitope was associated with the potential for metastasis, suggesting the importance of this epitope as a ligand for E-selectin. If the cimetidine given to the patients can efficiently block the expression of E-selectin on vascular endothelial cells, even malignant renal cell carcinoma cells expressing higher levels of sL^X would not be able to

adhere to the endothelium and the frequency of metastasis in the patients would be reduced, resulting in the beneficial effects for the patient survival. Taken together, these results suggested a beneficial effect of cimetidine on renal cell carcinoma patients, presumably by blocking the expression of E-selectin on vascular endothelial cells and inhibiting the adhesion of cancer cells. Future studies should clarify the effect of cimetidine on renal cell carcinoma with a high level of sL^X expression.

REFERENCES

1. Tozawa K, Sakurada S, Kohri K, *et al*: Effects of anti-nuclear factor κB reagents in blocking adhesion of human cancer cells to vascular endothelial cells. *Cancer Res* 55:4162–4167, 1995
2. Matsumoto S, Imaeda Y, Umemoto S, *et al*: Cimetidine increases survival of colorectal cancer patients with high levels of sialyl Lewis-X and sialyl Lewis-A epitope expression on tumour cells. *Br J Cancer* 86:161–167, 2002
3. Matsusako T, Muramatsu H, Shirahama T, *et al*: Expression of a carbohydrate signal, sialyl dimeric Le^X antigen, is associated with metastatic potential of transitional cell carcinoma of the human urinary bladder. *Biochem Biophys Res Commun* 181:1218–1222, 1991
4. Wang QY, Wu SL, Chen JH, *et al*: Expression of Lewis antigens in human non-small cell pulmonary cancer and primary liver cancer with different pathological conditions. *J Exp Clin Cancer Res* 22:431–440, 2003
5. Sumikura S, Ishigami S, Natsugoe S, *et al*: Disseminated cancer cells in the blood and expression of sialylated antigen in gastric cancer. *Cancer Lett* 200:77–83, 2003.
6. Paganuzzi M, Bobbio B, Marroni P, *et al*: Prognostic role of serum sialyl Lewis x (CD15s) in colorectal cancer. *Oncology* 65:52–59, 2003
7. Cordon-Cardo C, Reuter VE, Finstad CL, *et al*: Blood group-related antigens in human kidney: Modulation of Lewis determinants in renal cell carcinoma. *Cancer Res* 49:212–218, 1989
8. Kinouchi T, Saiki S, Maeda O, *et al*: Treatment of advanced renal cell carcinoma with a combination of human lymphoblastoid interferon-α and cimetidine. *J Urol* 157:1604–1607, 1997
9. Kobayashi K, Matsumoto S, Morishima T, *et al*: Cimetidine inhibits cancer cell adhesion to endothelial cells and prevents metastasis by blocking E-selectin expression. *Cancer Res* 60:3978–3984, 2000
10. Tozawa K, Akita H, Kawai N, *et al*: KAI1 expression can be a predictor of stage A prostate cancer progression. *Prostate Cancer Prostatic Dis* 4:150–153, 2001
11. Adams WJ, Morris DL: Short-course cimetidine and survival with colorectal cancer. *Lancet* 344:1768–1769, 1994
12. Matsumoto S: Cimetidine and survival with colorectal cancer. *Lancet* 346:115, 1992
13. Reynolds JL, Akhter J, Morris DL: In vitro effect of histamine and histamine H_1 and H_2 receptor antagonists on cellular proloferation of human malignant melanoma cell lines. *Melanoma Res* 6:95–99, 1996
14. Kimura E, Koike T, Shimizu Y: Complexes of histamine H_2-antagonist cimetidine with divalent and monovalent copperions. *Inorg Chem* 25:2242–2246, 1986
15. Hansbrough JF, Zapata-Sirvent RL, Bender EM: Prevention of alterations in postoperative lymphocyte subpopulations by cimetidine and ibuprofen. *Am J Surg* 151:249–255, 1986
16. Katoh J, Tsuchiya K, Sato W, *et al*: Cimetidine and immunoreactivity. *Lancet* 348:404–405, 1996
17. Srinivas U, Pahlsson P, Lundblad A: E-selectin: Sialyl Lewis, a dependent adhesion of colon cancer cells is inhibited differently by antibodies against E-selectin ligands. *Scand J Immunol* 44:197–203, 1996
18. Kawarada Y, Ishikura H, Kishimoto T, *et al*: The role of sialylated Lewis antigens on hematogeneous metastases of human pancreas carcinoma cell lines in vivo. *Pathol Res Pract* 196:259–263, 2000
19. Steinbach F, Tanabe K, Alexander ME, *et al*: The influence of cytokines on the adhesion of renal cancer cells to endothelium. *J Urol* 155:743–748, 1996
20. Caivano M: Role of MAP kinase cascades in inducing arginine transporters and nitric oxide synthetase in RAW264 macrophages. *FEBS Lett* 429:249–253, 1998
21. Miyazawa K, Mori A, Miyata H, *et al*: Regulation of interleukin-1 β-induced interleukin-6 gene expression in human fibroblast-like synoviocytes by p38 mitogen-activated protein kinase. *J Biol Chem* 273:24832–24838, 1998
22. Yang J-L, Ow KT, Ham JM, *et al*: Higher expression of oncoproteins c-myc, c-erb B/neu, PCNA and p53 in metastasizing tumors. *Ann Surg Oncol* 3:574–579, 1996
23. Read MA, Whitley MZ, Gupta S, *et al*: Tumor necrosis factor α-induced E-selectin expression is activated by the nuclear factor-κB and c-JUN N-terminal kinase/p38 mitogen-activated protein kinase pathway. *J Biol Chem* 272:2753–2761, 1997
24. Pietersma A, Tilly BC, Gaestel M, *et al*: P38 mitogen activated protein kinase regulates endothelial VCAM-1 expression at the post-transcriptional level. *Biochem Biophys Res Commun* 230:44–48, 1997
25. Majuri ML, Niemela R, Tiisala S, *et al*: Expression and function of α 2,3-sialyl-and α 1,3/1,4-fucosyltransferases in colon adenocarcinoma cell lines: Role in synthesis of E-selectin counter-receptors. *Int J Cancer* 63:551–559, 1995

Growth Inhibition of Multiple Myeloma Cells by a Novel IκB Kinase Inhibitor

Takaomi Sanda,[1,2] Shinsuke Iida,[2] Hiroka Ogura,[1] Kaori Asamitsu,[1] Toshiki Murata,[3] Kevin B. Bacon,[4] Ryuzo Ueda,[2] and Takashi Okamoto[1]

Departments of [1]Molecular and Cellular Biology, and [2]Internal Medicine and Molecular Science, Nagoya City University Graduate School of Medical Sciences, Nagoya, Japan and Departments of [3]Chemistry and [4]Biology, Research Center Kyoto, Bayer Yakuhin, Ltd., Kyoto, Japan

ABSTRACT

Involvement of nuclear factor-κB (NF-κB) in cell survival and proliferation of multiple myeloma has been well established. In this study we observed that NF-κB is constitutively activated in all human myeloma cell lines, thus confirming the previous studies. In addition, we found the phosphorylation of p65 subunit of NF-κB in addition to the phosphorylation of IκBα and the activation of NF-κB DNA binding and that various target genes of NF-κB including *bcl-x_L*, *XIAP*, *c-IAP1*, *cyclin D1*, and *IL-6* are up-regulated. We then examined the effect of a novel IκB kinase inhibitor, 2-amino-6-[2-(cyclopropylmethoxy)-6-hydroxyphenyl]-4-piperidin-4-yl nicotinonitrile (ACHP). When myeloma cells were treated with ACHP, the cell growth was efficiently inhibited with IC_{50} values ranging from 18 to 35 μmol/L concomitantly with inhibition of the phosphorylation of IκBα/p65 and NF-κB DNA-binding, down-regulation of the NF-κB target genes, and induction of apoptosis. In addition, we observed the treatment of ACHP augmented the cytotoxic effects of vincristine and melphalan (L-phenylalanine mustard), conventional antimyeloma drugs. These findings indicate that IκB kinase inhibitors such as ACHP can sensitize myeloma cells to the cytotoxic effects of chemotherapeutic agents by blocking the antiapoptotic nature of myeloma cells endowed by the constitutive activation of NF-κB.

INTRODUCTION

Multiple myeloma is an intractable B-cell malignancy characterized by clonal proliferation of a terminally differentiated plasma cell in bone marrow associated with monoclonal hypergammaglobulinemia and multiple osteolytic bone lesions (1, 2). Although recent combination chemotherapy, using melphalan [L-phenylalanine mustard (PAM)], vincristine, and corticosteroids, can induce complete remission in multiple myeloma patients, the long-term remission is hardly attainable mostly due to the frequent acquisition of drug resistance and low adherence (1). Therefore, novel treatment modality has been intensively investigated.

It is noted that the interaction between myeloma cells and bone marrow stromal cells plays a crucial role through the production of cytokines or growth factors and the cognate binding of adhesion molecules (1). Among various cytokines and growth factors, interleukin-6 (IL-6) and vascular endothelial growth factor were reported to stimulate myeloma cell proliferation and its migration (3). The establishment of such bone marrow microenvironment conceivably accelerates cell proliferation. In other words, a limited number of genes including IL-6, vascular endothelial growth factor, and adhesion molecules are the principal pathophysiologic determinants of multiple myeloma. Interestingly, gene expression of these genes is under the control of a common transcription factor, nuclear factor-κB (NF-κB; refs. 1, 4). Moreover, extracellular stimuli for the growth of myeloma cells, such as CD40 ligand (CD40L) expressed on activated T cells, insulin-like growth factor I, and tumor necrosis factor α (TNFα), are known to promote the NF-κB activation pathway at various steps (5–7). A similar effect of NF-κB is also noted in other malignancies including adult T-cell leukemia (8), chronic lymphocytic leukemia (9), activated B-cell diffuse large B-cell lymphoma (9), Hodgkin's disease (9), hepatocellular carcinoma (10), and colorectal cancer (11). In fact, NF-κB inhibitors were found effective in the treatment of some cancers (12). Thus, NF-κB and its signal transduction pathway are considered as the feasible molecular target for novel cancer therapy.

NF-κB is a hetero- or homodimer consisting of Rel family proteins, p65 (RelA), RelB, c-Rel, p50/p105, and p52/p100, and normally present in the cytoplasm in association with its inhibitor, IκB (13). Stimulation by the inflammatory cytokines such as TNFα and IL-1β results in the activation of IκB kinase (IKK) complex through mitogen-activated protein kinase/extracellular signal-regulated kinase kinase kinase 1,3 or NF-κB-inducing kinase (14, 15). IKK is a large molecular weight complex consisting of three subunits, IKKα, IKKβ, and IKKγ/NEMO, in which IKKα and IKKβ serve as catalytic subunits that phosphorylate IκBα on two serine residues (Ser32/Ser36; refs. 16–18). Recent reports by us and others have shown that IKKα also phosphorylates p65 at Ser536, which is crucial for the transcriptional competence of NF-κB when bound to the promoter sequence of target genes in the nucleus (19, 20).

In this study, we examined the effect of a novel IKK inhibitor, 2-amino-6-[2-(cyclopropylmethoxy)-6-hydroxyphenyl]-4-piperidin-4-yl nicotinonitrile (ACHP), on the growth and survival of myeloma cell lines. This compound was initially

Received 9/22/04; revised 11/19/04; accepted 12/6/04.
Grant support: Ministry of Education, Culture, Sports, Science, and Technology, and the Ministry of Health, Labor, and Welfare of Japan. The costs of publication of this article were defrayed in part by the payment of page charges. This article must therefore be hereby marked *advertisement* in accordance with 18 U.S.C. Section 1734 solely to indicate this fact.
Requests for reprints: Takashi Okamoto, Department of Molecular and Cellular Biology, Nagoya City University Graduate School of Medical Sciences, 1 Kawasumi, Mizuho-cho, Mizuho-ku, Nagoya, Aichi 467-08601, Japan. Phone: 81-52-853-8205; Fax: 81-52-859-1235; E-mail: tokamoto@med.nagoya-cu.ac.jp.

synthesized by Murata et al. (21) based on the massive screening. Among these compounds, ACHP exhibited the highest selectivity for IKKβ and IKKα (IC_{50} values for IKKβ and IKKα are 8.5 and 250 nmol/L, respectively, measured by *in vitro* kinase assays) over other kinases such as IKK3, Syk, and mitogen-activated protein kinase kinase kinase 4 (IC_{50} > 20 μmol/L for these kinases; ref. 22). In addition, ACHP showed good aqueous solubility and cell-permeability, thus demonstrating a very high oral bioavailability in mice and rats.

Here we show that IκBα and p65 are constitutively phosphorylated in myeloma cells, indicating the persistent activation of NF-κB, and ACHP could efficiently block NF-κB pathway in myeloma cells, thus arresting cell growth and inducing apoptotic cell death. An apparent synergism was also detected between ACHP and other conventional anticancer drugs used in the treatment of myeloma.

MATERIALS AND METHODS

Cell Lines. Human myeloma cell lines, ILKM-2, ILKM-3, KM5, U266, NCUMM-2, AMO1, and NOP1, and a B-cell lymphoma cell line, BJAB, were used in this study as described previously (23). These cell lines were cultured in RPMI 1640 supplemented with 10% fetal bovine serum, streptomycin, and penicillin at 37°C in 5% CO_2 incubator. Exogenous IL-6 is required for the growth of ILKM-2 and ILKM-3, whereas other cell lines can grow without exogenous IL-6. U266 cells produce IL-6 in an autocrine fashion. Although U266 and BJAB cells are known to have constitutively activated NF-κB (24, 25), constitutive activation of NF-κB has not been definitively reported in other cell lines.

Reagents. The novel IKK inhibitor, ACHP, was a kind gift from Bayer Yakuhin (Kyoto, Japan). Melphalan (PAM), vincristine, and dexamethasone were obtained from Sigma (St. Louis, MO). PAM was dissolved in dimethyl sulfoxide whereas vincristine and dexamethasone were resolved in PBS. In each experiment, equal amounts of dimethyl sulfoxide or PBS were added to control cells. We confirmed that dimethyl sulfoxide concentrations used in this study did not affect cell viability (data not shown). Human recombinant TNFα was purchased from Roche (Mannheim, Germany) and used at 5 ng/mL for NF-κB stimulation. Recombinant human IL-6 (Diaclone Reseach, Basaon, France) was added at a final concentration of 10 ng/mL.

Immunoblot Analysis. For analysis of various proteins, ~ 1.0×10^6 cells were maintained with or without ACHP at 37°C. These cells were washed once with cold PBS and resuspended in 50 μL of hypotonic lysis buffer [20 mmol/L HEPES-KOH (pH 7.9), 10 mmol/L KCl, 1 mmol/L EDTA, 1 mmol/L Na_3VO_4, 5 mmol/L NaF, 1 mmol/L phenylmethylsulfonyl fluoride, 0.2% Triton X-100, protease inhibitor]. After 20 minutes of incubation on ice, the samples were centrifuged and the supernatant was collected as cytoplasmic extract. Protein concentration was measured using detergent-compatible protein assay (Bio-Rad, Hercules, CA) and equal amounts of the proteins were electrophoresed on 10% SDS-PAGE and transferred onto the nitrocellulose membrane. The membranes were blocked with TBS-T [10 mmol/L Tris-HCl (pH 8.0), 15 mmol/L NaCl, 0.1% Tween 20] containing 5% nonfat milk for 2 hours at room temperature, and incubated with TBS-T containing 5% nonfat milk and 1:1,000 diluted antibodies against either phospho-IκB-α (Ser32) or phospho-p65 (Ser536; Cell Signaling Technology, Beverly, MA) overnight at 4°C. For antibodies against p65, p52/p100, IκB-α, and α-tubulin (Santa Cruz, Santa Cruz, CA), incubation was done at room temperature for 2 hours. After incubation, the membranes were rinsed with TBS-T and further incubated with horseradish peroxidase-conjugated secondary antibodies (Amersham Biosciences, Buckinghamshire, United Kingdom) in TBS-T with 5% nonfat milk at room temperature for 1 hour. Each protein was detected by chemiluminescence using SuperSignal (Pierce, Rockford, IL).

Electrophoretic Mobility Shift Assay. Electrophoretic mobility shift assay was done as described previously (26). Briefly, 1.0×10^6 cells were cultured with or without ACHP at 37°C, washed with PBS, and treated with hypotonic lysis buffer. After 20 minutes of incubation on ice, the cells were centrifuged to remove supernatant and resuspended in 50 μL of hypertonic lysis buffer [50 mmol/L HEPES-KOH (pH 7.9), 400 mmol/L NaCl, 1 mmol/L EDTA, 1 mmol/L Na_3VO_4, 5 mmol/L NaF, 1 mmol/L phenylmethylsulfonyl fluoride, 0.2% Triton X-100, protease inhibitor]. Thirty minutes after incubation at 4°C, the supernatant was collected as nuclear extract. Electrophoretic mobility shift assay was done using double stranded oligonucleotides containing the κB sequence taken from HIV long terminal repeat (5′-TGT CGA ATG CAA ATC ACT AGA A-3′). The probe DNA was 5′ end-labeled using T4 polynucleotide kinase and [γ-^{32}P]-ATP (Amersham Biosciences). DNA binding reactions were done at 30°C for 15 minutes with labeled DNA and 25 μg nuclear extract in 20 μL binding buffer [22 mmol/L HEPES-KOH (pH 7.9), 80 mmol/L KCl, 5% glycerol, 0.1% NP40, 1 mmol/L DTT, 2 μg poly dI-dC, 2 μg tRNA, and protease inhibitor]. The samples were loaded on 5% non-denaturing polyacrylamide gel with 0.5× Tris-Borate-EDTA buffer at 4°C, followed by autoradiography.

Transient Luciferase Assay. Approximately 2.0×10^6/well U266 cells were transfected in 12-well plates in triplicates using DEMRIE-C reagent (Invitrogen, Carlsbad, CA) according to the recommendation of the manufacturer. For each transfection, 2.5 μg of reporter plasmid, 4κBwt-Luc, or 4κBmut-Luc, and 1.5 μg of the internal control plasmid, pRL-TK, expressing Renilla luciferase, were used. The construction of these plasmids was described previously (26). Twenty-four hours after transfection, the cells were treated with ACHP. After 4 hours of incubation, the cells were harvested and the luciferase activity was measured by luminometer as described (27). The cells were treated with TNFα and harvested after 30 minutes of treatment. The luciferase activity was normalized with Renilla luciferase activity used as an internal control. The efficiency of transfection was about 0.9% as estimated from the experiment with a plasmid expressing green fluorescent protein (data not shown).

Reverse Transcription-PCR. To detect mRNA expression of various genes, 1.0×10^6 cells in 1 mL were maintained at 37°C in CO_2 incubator, washed once with PBS, homogenized with QIAshredder (Qiagen, Alameda, CA), and total RNA was purified using RNeasy (Qiagen) according to the protocol of the manufacturer. After incubation with DNase I (Invitrogen), 1 μg of total RNA was reverse transcribed using SuperScript First-Strand synthesis System (Invitrogen). One-seventh of each sample was subjected to PCR amplification for 33 cycles, and the products

were analyzed by agarose gel electrophoresis. The oligonucleotideprimers were as follows: *bcl-2*, sense 5′-TCG CTA CCG TCG TGA CTT C-3′ and antisense, 5′-AAA CAG AGG TCG CAT GCT G-3′; *bcl-x_L*, sense 5′-GTT GTA CCT GCT TGC TGT CGC CGG-3′ and antisense 5′-AGC TTG TAG GAG AGA AAG TCG ACC-3′; *cyclin D1*, sense 5′-CCC TCG GTG TCC TAC TTC AAA-3′ and antisense 5′-CAC CTC CTC CTC CTC CTC TTC-3′; *XIAP*, sense 5′-CTT GCA TAC TGT CTT TCT GAG C-3′ and antisense, 5′-ACA CCA TAT ACC CGA GGA AC-3′; *c-IAP1*, sense 5′-CCT GTG GTT AAA TCT GCC TTG-3′ and antisense 5′-CAA TTC GGC ACC ATA ACT CTG-3′; *β-actin*, sense CCA GGC ACC AGG GCG TGA TG-3′ and antisense 5′-CGG CCA GCC AGG TCC AGA CG-3′.

Interleukin-6 Production Assay. To measure IL-6 production, 2.0×10^5 of U266 cells in 500 μL medium were cultured at 37°C for 48 hours, centrifuged to collect supernatant, and the IL-6 concentrations were determined using ELISA kit according to the instruction of the manufacturer (Amersham Biosciences).

Growth Inhibition Assay. Growth inhibitory effects of compounds were analyzed using 3-(4,5-dimethylthiazol-2-yl)-2,5-diphenyltetrazolium bromide assay (27). Approximately 1.0×10^4 to 1.5×10^4 cells (in 100 μL/well) were cultured in 96-well plates in triplicates in the presence or absence of each reagent or in combination at 37°C. After incubation, 10 μL (5 mg/mL) of 3-(4,5-dimethylthiazol-2-yl)-2,5-diphenyltetrazolium bromide solution (Sigma) were added to each well, the cells were incubated for 4 hours at 37°C, and 100 μL of lysis buffer (0.04 mol/L HCl, isopropanol) were added. Absorbances at 570 and 630 nm were measured with the aid of multiplate reader using plain medium as blank. Cell viability (%) was calculated as follows: ($A_{630} - A_{570}$ of the samples / $A_{630} - A_{570}$ of the control) × 100 (%).

Cell Cycle Analysis. Cytofluorometric analysis was done with $\sim 1.0 \times 10^6$ cells as previously described (28). After incubation with or without ACHP, the cells were washed with cold PBS and fixed with 70% ethanol at −30°C overnight. The cell pellets were resuspended in 500 μL PBS containing 2 mg/mL RNase A (Roche) and kept at 37°C for 30 minutes. Then, the cell pellets were resuspended in 500 μL PBS containing 20 mg/mL propiodium iodide (PI) followed by incubation at room temperature for 30 minutes. The DNA content of each cell preparation was analyzed by flow cytometry (FACScan, BD Bioscience, San Jose, CA) using CellQuest analysis program.

Apoptosis Assay. Briefly, cells undergoing apoptosis were detected as previously reported (29). After treating the cells (2.0×10^5 cells) at 37°C with or without ACHP for 8 hours, the cells were washed with cold PBS and resuspended in staining buffer containing PI and FITC-conjugated Annexin V (MEBCYTO apoptosis kit, MBL, Nagoya, Japan). After 20 minutes of incubation in the dark at room temperature, the cells were analyzed by flow cytometry.

RESULTS

Constitutive Phosphorylation of IκBα and p65 in Myeloma Cell Lines. In order to see the status of NF-κB signaling in myeloma cells, we examined the phosphorylation of IκBα and p65 subunit in a number of myeloma cell lines and BJAB B-cell line. As shown in Fig. 1, the phosphorylation of IκBα at Ser32 was detected in most of the cell lines examined, especially in U266, ILKM-2, NCUMM-2, and BJAB. The upper bands, corresponding to heavily phosphorylated IκBα, were detected in ILKM-2 and NCUMM-2. In addition, p65 is phosphorylated at Ser536 in all the cell lines examined. This constitutive phosphorylation of IκBα was observed even when cells were cultured in serum-free medium (data not shown). These findings suggest that NF-κB is constitutively activated in myeloma cells.

Constitutive Activation of Nuclear Factor-κB DNA Binding and Inhibition by 2-Amino-6-[2-(Cyclopropylmethoxy)-6-Hydroxyphenyl]-4-Piperidin-4-yl Nicotinonitrile. We then examined if NF-κB DNA-binding is constitutively activated in these myeloma cells by electrophoretic mobility shift assay. Representative results are shown in Fig. 2 with U266 and NCUMM-2 cells, in which the NF-κB DNA-binding is constitutively activated. We also examined the effect of ACHP on the NF-κB DNA binding in these cells and found that ACHP, specific inhibitor of IKKα and IKKβ, could inhibit the DNA binding activity of NF-κB (Fig. 2*B*). The inhibitory effect was observed at ACHP concentrations greater than 10 μmol/L, and was evident after only 4 hours of treatment with ACHP (Fig. 2*C*).

Inhibition of IκBα and p65 Phosphorylation by 2-Amino-6-[2-(Cyclopropylmethoxy)-6-Hydroxyphenyl]-4-Piperidin-4-yl Nicotinonitrile. We then examined the effect of ACHP on the phosphorylation of IκBα and p65. As shown in Fig. 3*A*, ACHP efficiently inhibited the phosphorylation of IκBα and p65 at 1 μmol/L, and phosphorylated forms of these proteins disappeared at higher concentrations. This inhibitory action was observed as early as 20 minutes after treatment (Fig. 3*B*). No effect of ACHP on the processing of p100/p52, another subunit of NF-κB, was observed. Similar effects of ACHP were observed with other myeloma cell lines (data not shown).

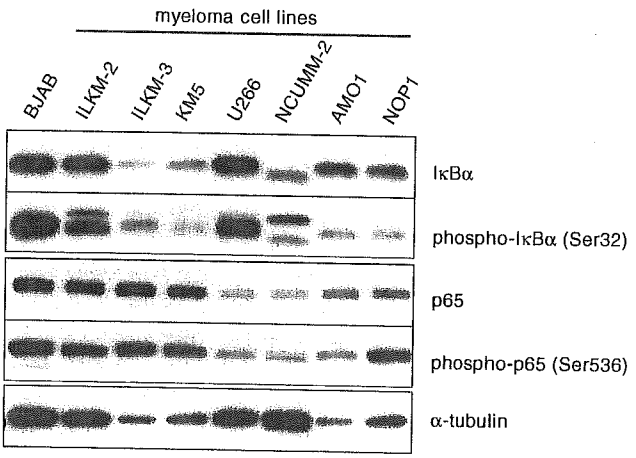

Fig. 1 Constitutive phosphorylation of IκBα and p65 in myeloma cell lines. The cytoplasmic extracts obtained from seven myeloma cell lines (U266, ILKM-2, NCUMM-2, ILKM-3, KM5, AMO1, and NOP1) and a B-cell line (BJAB), maintained in culture without any stimulation, were examined by Western blotting analyses with specific antibodies against IκBα, phospho-IκBα (at Ser32), p65, and phospho-p65 (at Ser536). Anti-α-tubulin antibody was used as an internal control. The mobility shift of the phosphorylated IκBα is noted in ILKM-2 and NCUMM-2 cells, suggesting phosphorylation at multiple sites.

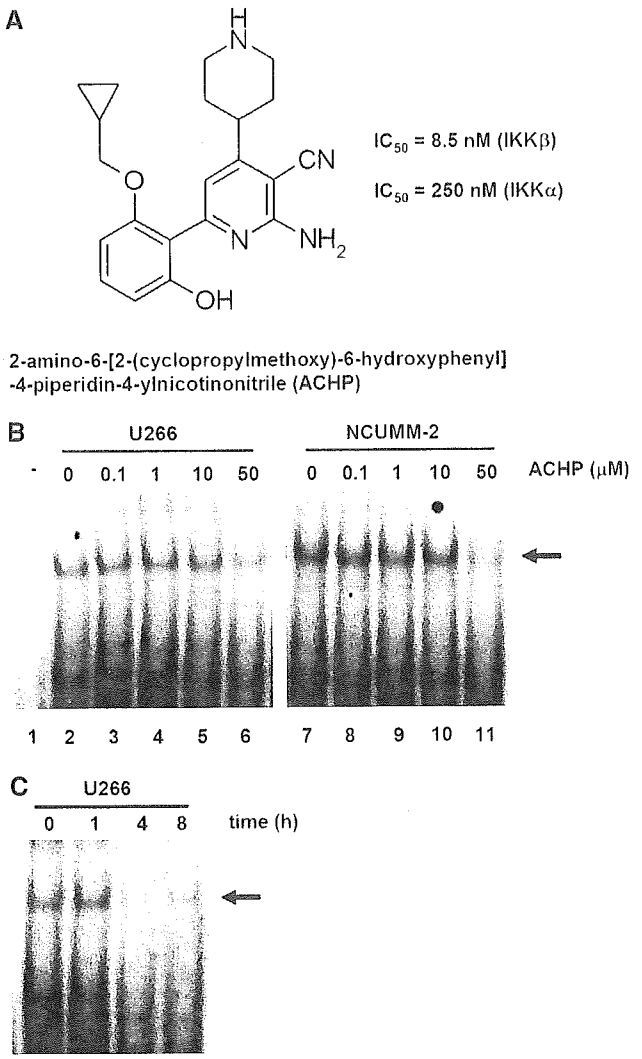

Fig. 2 Constitutive activation of NF-κB DNA binding in myeloma cells and inhibitory effect of ACHP. *A*, structure of ACHP. *B*, dose-dependent inhibition of NF-κB DNA binding by ACHP. The myeloma cell lines, U266 and NCUMM-2, were cultured in the absence of any stimulation and treated with ACHP (0-50 μmol/L) for 4 hours. Nuclear extracts were prepared and subjected to electrophoretic mobility shift assay. Arrow, location of the DNA-NF-κB complex, which was confirmed by the competition assay using unlabelled κB DNA probe and the supershift assay using antibodies for NF-κB subunits (data not shown). Lane 1, probe DNA only; lanes 2-6 and 7-11, fixed amounts (~25 μg) of nuclear extracts from U266 and NCUMM-2 cells, respectively, were incubated with the DNA probe. The indicated concentrations of ACHP were added in cell cultures for 4 hours before preparation of the nuclear extract. *C*, time-dependent inhibition of NF-κB DNA binding by ACHP. U266 cells were treated with ACHP (50 μmol/L) for 0 to 8 hours before preparation of the nuclear extract.

Effect of 2-Amino-6-[2-(Cyclopropylmethoxy)-6-Hydroxyphenyl]-4-Piperidin-4-yl Nicotinonitrile on the Tumor Necrosis Factor α–mediated Nuclear Factor-κB Transactivation. We then examined the inhibitory effect of ACHP on NF-κB transactivation activity. By transfection of NF-κB-dependent luciferase reporter plasmid to U266 cells, ~4-fold increase in the extent of gene expression was observed (Fig. 4*A*). When cells were pretreated with ACHP 4 hours before the stimulation with TNFα, a dose-dependent inhibition of gene expression was observed. The inhibitory action was evident at 0.1 μmol/L ACHP. No such effect of ACHP was observed in control transcription using a reporter plasmid devoid of NF-κB binding sites.

Inhibition of Gene Expressions of *cyclin D1*, *bcl-x_L*, *XIAP*, and *c-IAP1* by 2-Amino-6-[2-(Cyclopropylmethoxy)-6-Hydroxyphenyl]-4-Piperidin-4-yl Nicotinonitrile. In myeloma cells, constitutive NF-B activation and transcriptional induction of target antiapoptotic genes such as *bcl-x_L*, *XIAP*, and *c-IAPs* are ascribable to the resistance to apoptotic stimuli by anticancer agents (30, 31). In addition, NF-B also contributes to cell proliferation of myeloma cells by up-regulating growth-promoting genes such as *cyclin D1* (30). We thus examined the effect of ACHP on gene expression of these genes. As shown in Fig. 4*B*, whereas gene expression levels of β-*actin* (control) were not changed by the treatment of U266 with ACHP, inhibition of gene expressions of *bcl-x_L*, *XIAP*, *c-IAP1*, and *cyclin D1*

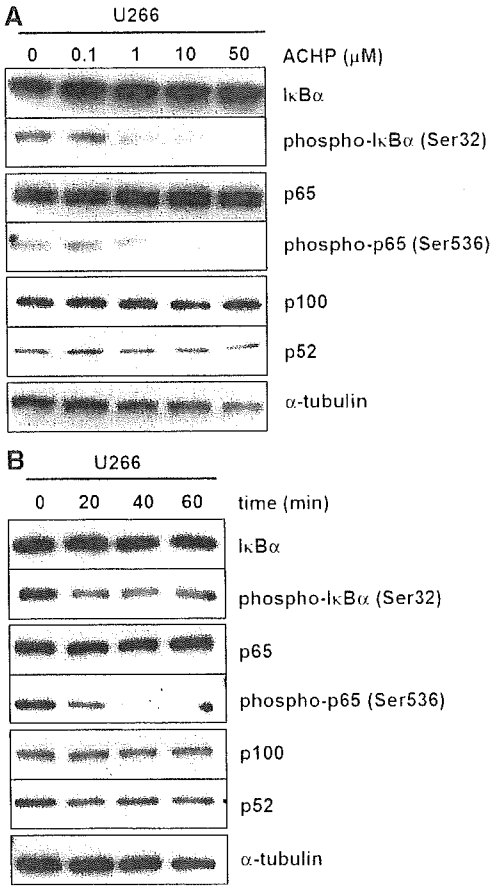

Fig. 3 Inhibition of IκBα and p65 phosphorylation by ACHP. *A*, dose-dependent inhibition by ACHP. U266 cells were treated with ACHP (0-50 μmol/L) for 20 minutes. Cytoplasmic extracts were prepared and subjected to immunoblots with the indicated antibodies. The IC_{50} values for phospho-IκBα and phospho-p65 were 1.0 and 7.6 μmol/L, respectively. *B*, time-dependent inhibition of IκBα and p65 phosphorylation by ACHP. U266 cells were treated with ACHP (10 μmol/L) for 0 to 60 minutes and the nuclear extract was obtained for the immunoblot analyses.

was observed. The expression of *bcl-2* was not remarkably affected by ACHP. The inhibitory action of ACHP was observed after 4 hours (Fig. 4*C*). Similar results were observed with NCUMM-2 and ILKM-2 cells (data not shown). Moreover, the effect of ACHP on the production of a growth promoting cytokine, IL-6, was examined with IL-6-secreting myeloma cell line, U266. As shown in Fig. 4*D*, a significant reduction of IL-6 was evident at concentrations of ACHP greater than 0.1 mol/L. Increasing concentration of ACHP resulted in further reduction of IL-6 production associated with repression of cell growth.

Suppression of Cell Cycle Progression and Induction of Apoptosis by 2-Amino-6-[2-(Cyclopropylmethoxy)-6-Hydroxyphenyl]-4-Piperidin-4-yl Nicotinonitrile. When U266 and NCUMM-2 cells were treated with 10 μmol/L ACHP for 24 hours, cell cycle progression was affected. As shown in Fig. 5*A*, whereas 24% of U266 cells were at S phase, only 17.0% of U266 cells were at S phase after treatment with ACHP. Similar results were obtained with NCUMM-2 cells. ACHP also induced apoptosis in myeloma cell lines. In Fig. 5*B*, the number of cells undergoing apoptosis (Annexin V (+) and PI (−)) was measured. Although the sensitivity of apoptosis to ACHP varied among different cell lines, ACHP could efficiently induce cell death. For example, in U266 cells, which were relatively resistant to the ACHP-induced apoptosis, 50 μmol/L ACHP treatment increased the fraction of apoptotic cells from 4.2% (no treatment) to 16.0%. In NCUMM-2 cells, even a lower concentration of ACHP (10 μmol/L) could efficiently induce apoptosis (15.8%) and a higher concentration of ACHP (50 μmol/L) induced apoptosis in 43.7% of the cells. These findings illustrate the effect of ACHP in down-regulating antiapoptotic genes (Fig. 4).

Growth Inhibitory Effects of 2-Amino-6-[2-(Cyclopropylmethoxy)-6-Hydroxyphenyl]-4-Piperidin-4-yl Nicotinonitrile. We then assessed the net effects of ACHP on the growth of myeloma cell lines (U266, NCUMM-2, and ILKM-2) and B-cell line (BJAB). As shown in Fig. 6*A*, ACHP inhibited cell growth in a dose-dependent manner with mean IC_{50} of 26.8 μmol/L in three myeloma cell lines. There was a sharp decline in cell growth property between 10 and 50 μmol/L of ACHP in most of the cells, which corresponded with the effective ACHP concentration that inhibited expression of antiapoptotic genes (Fig. 4). Figure 6*B* shows the time course of cell growth property of U266 cells with various concentrations of ACHP. Higher concentrations of ACHP were necessary to inhibit cell growth. Lower ACHP concentrations (10 μmol/L and below) eventually allowed myeloma cells to grow for a longer time. Similar observations were obtained with other myeloma cells examined (data not shown).

Effects of 2-Amino-6-[2-(Cyclopropylmethoxy)-6-Hydroxyphenyl]-4-Piperidin-4-yl Nicotinonitrile with Other Antimyeloma Agents. Finally, we examined the feasibility of ACHP as an adjuvant chemotherapeutic agent in myeloma treatment. In the experiments described in Fig. 6*C*, U266 cells were cultured in the presence of PAM, vincristine, and dexamethasone together with ACHP and the effects on cell growth were assessed. Although 10 μmol/L of ACHP alone did not efficiently inhibit U266 cell growth (Fig. 6*A*), combination with either PAM, vincristine, or dexamethasone showed more

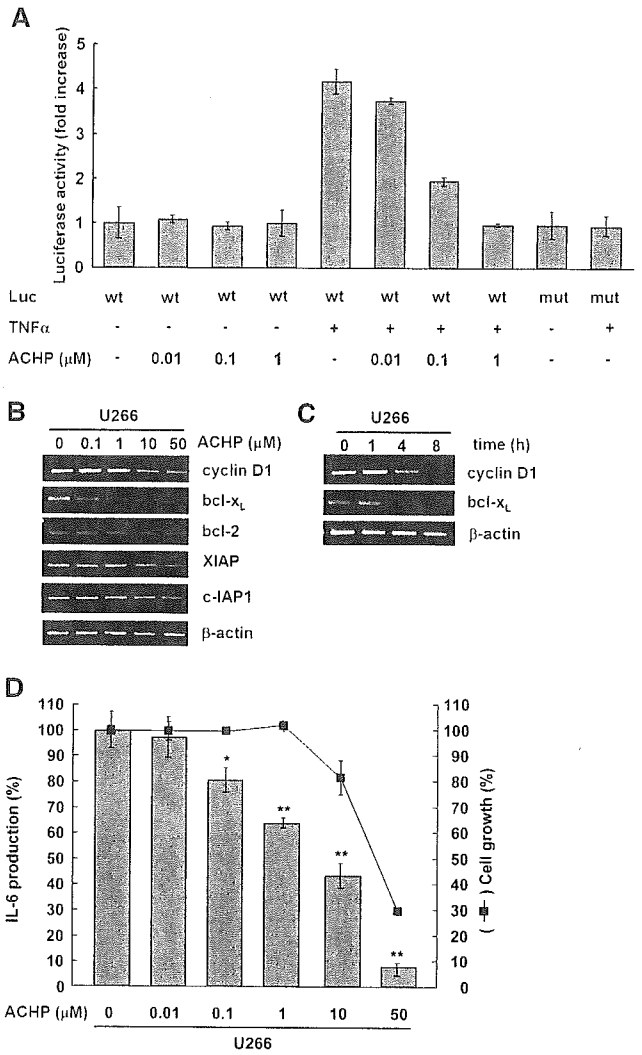

Fig. 4 Inhibition of the NF-κB dependent transactivation and gene expression by ACHP. Luciferase reporter plasmid containing wild-type NF-κB binding sequence (*wt*) or its mutant (*mut*) was transfected into U266 cells together with an internal control plasmid (pRL-TK). Forty hours after transfection, the cells were treated with ACHP (0-1 μmol/L) for 4 hours, stimulated by TNFα (5 μg/mL) for 30 minutes, and harvested for luciferase assay. The luciferase activity is indicated as fold increase compared with the untreated control (=1.0). Transfection efficiency was ~0.9% as evaluated by green fluorescent protein assay (data not shown). Experiments were done in triplicates; columns, mean; bars, SD. *B*, dose-dependent inhibition by ACHP. After U266 cells were treated with ACHP (0-50 μmol/L) for 4 hours, total RNA samples were prepared for reverse transcription-PCR, and the mRNA levels of *cyclin D1*, *bcl-xL*, *bcl-2*, *XIAP*, *c-IAP1*, and *β-actin* were examined with specific primers. *C*, time-dependent inhibition by ACHP. U266 cells were treated with ACHP (50 μmol/L) for 0 to 8 hours, total RNA samples were prepared, and the mRNA level of each gene was assessed by reverse transcription-PCR. *D*, down-regulation of IL-6 production by ACHP. U266 cells were incubated in the presence of ACHP (0-50 μmol/L) for 48 hours and the IL-6 levels in the supernatant were measured by ELISA method (*solid bar*). The effect of ACHP on the net cell growth was examined by 3-(4,5-dimethylthiazol-2-yl)-2,5-diphenyltetrazolium bromide assay (*square*). The results are expressed as percentage compared with the untreated control. Experiments were done in triplicates; columns, mean; bars, SD. *, $P = 0.05$; **, $P < 0.01$.

than additive effects in blocking cell growth in a dose-dependent manner (Fig. 6*C*). When cell cultures were maintained for up to 5 days, a greater effect was observed with vincristine and ACHP (Fig. 6*D*). Although similar effects were observed with PAM and ACHP for the first 3 days, the synergistic effect was diminished after 5 days, presumably due to the short half-life of PAM.

DISCUSSION

In spite of a significant advancement in conventional chemotherapy and wider applicability of high-dose treatment with transplantation of hematopoietic stem cells, multiple mye loma still remains incurable (3). Thus, the pursuit for novel therapeutic modalities has been attempted by many laboratories. One such approach is the chemotherapeutic intervention of the NF-κB activation cascade (25, 32–34). In this study, we examined the effect of ACHP, a newly developed IKK inhibitor, on the growth of myeloma cells. We confirmed the previous observations of Bharti et al. (25, 35) that NF-κB is constitutively activated in myeloma cells and found that ACHP could effectively inhibit the myeloma cell growth. We also found that the cell growth inhibitory effect of conventional antimyeloma compounds, vincristine and PAM, was significantly augmented when combined with ACHP. These findings support the idea that NF-κB could be a feasible molecular target for the treatment of multiple myeloma.

Regarding the mechanism by which NF-κB is activated in myeloma cells, we found the constitutive phosphorylation of p65 subunit of NF-κB at Ser536 as well as that of IκBα at Ser32. Although the constitutive phosphorylation of IκBα at Ser32 has been reported in myeloma cells (25, 35), the constitutive phosphorylation of p65 has not been explored. There are at least three phosphorylation sites, Ser276, Ser529, and Ser536, within p65. Among these phosphorylation sites of p65, Ser536 phosphorylation plays crucial roles in the NF-κB-mediated transactivation (36). For example, the point mutation of Ser536

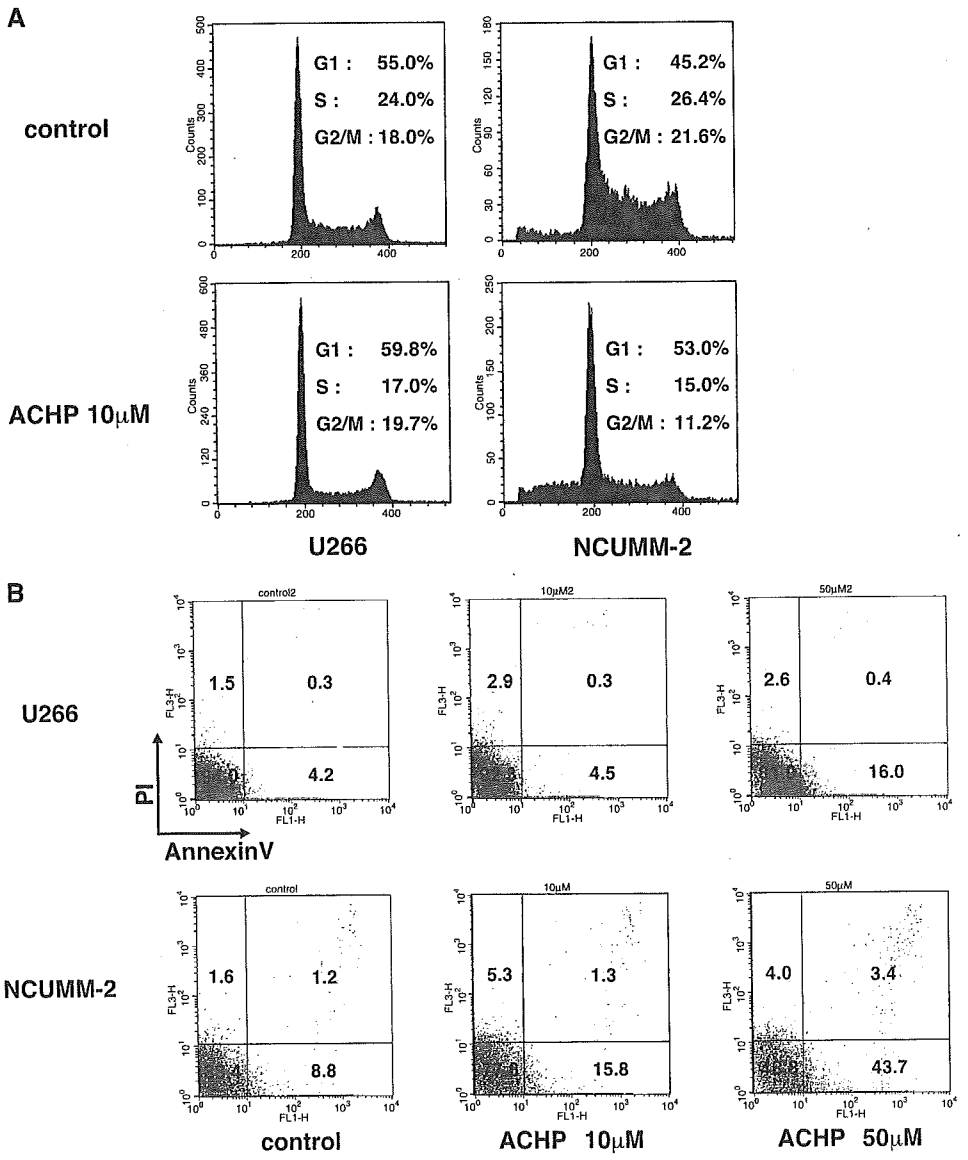

Fig. 5 Effects of ACHP on cell cycle and induction of apoptosis. *A*, inhibition of cell cycle progression by ACHP. U266 and NCUMM-2 cells were treated with ACHP (10 μmol/L) for 24 hours. Cells were stained with PI and subjected to flow cytometric analysis. The fractions of each cell cycle phase (%) are shown as percentage using the CellQuest analysis program. *B*, induction of apoptotic cells by ACHP. U266 and NCUMM-2 cells were treated with ACHP (0, 10, and 50 μmol/L) for 8 hours, stained with FITC-conjugated Annexin V and PI, and analyzed by flow cytometry. Normal cells do not stain with Annexin V or PI, whereas apoptotic cells stain with Annexin V but not PI. The percentage of each fraction is indicated.

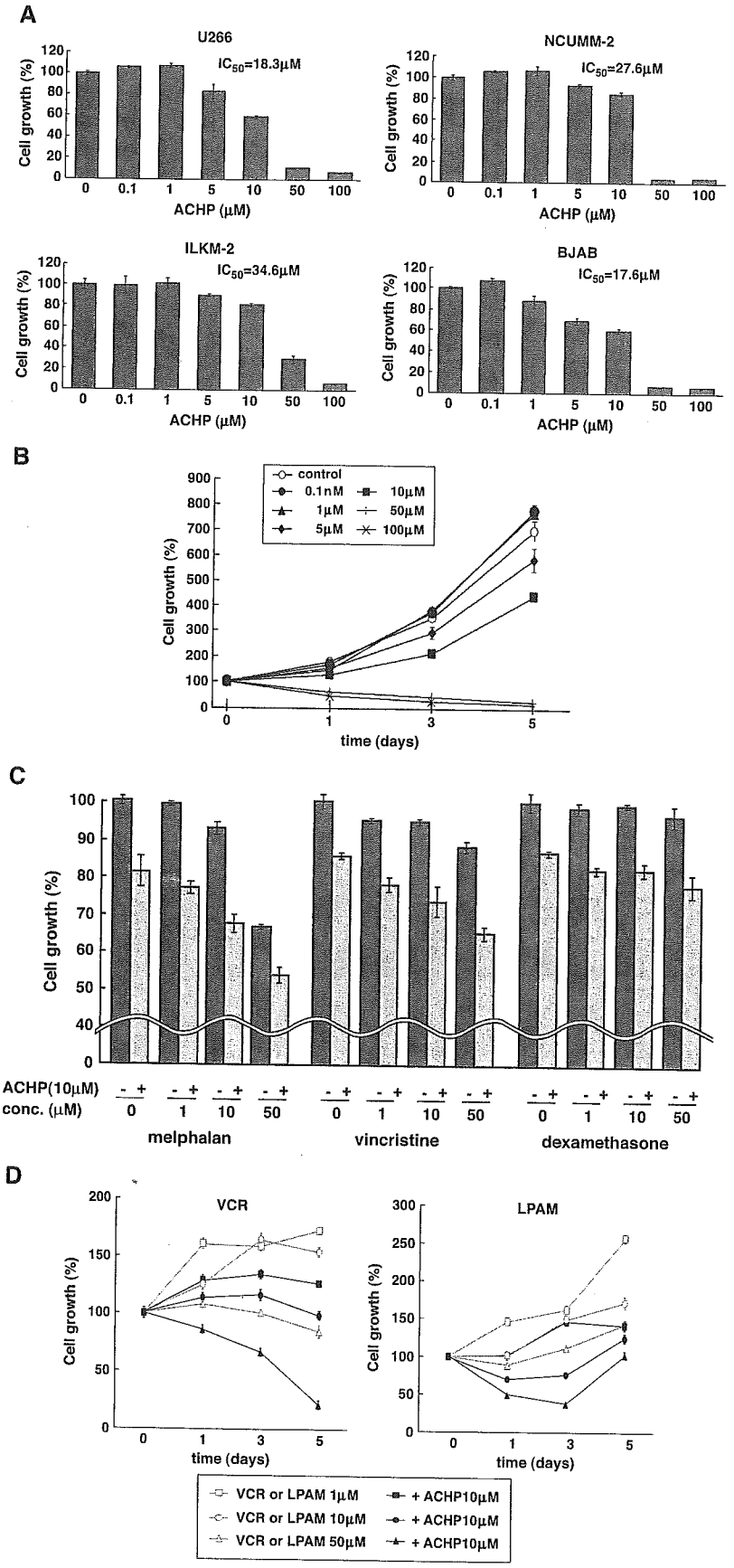

Fig. 6 Growth inhibitory effects of ACHP. Cell growth was monitored by 3-(4,5-dimethylthiazol-2-yl)-2,5-diphenyltetrazolium bromide assay. The results are indicated as percentage compared with the untreated control or day 0. Experiments were done in triplicates; columns, mean; bars, SD. *A,* cell growth analysis of myeloma cell lines and the inhibitory effects of ACHP. Each myeloma cell and BJAB was treated with the indicated concentrations of ACHP for 3 days. *B,* effects of ACHP on the temporal profiles of U266 cell growth. U266 cells were treated with indicated concentrations of ACHP (0-100 μmol/L) up to 5 days. *C,* synergistic effects of ACHP with other antimyeloma agents. The U266 myeloma cells were cultured with indicated concentrations of antimyeloma agents in the absence or presence (10 μmol/L) of ACHP for 1 day. *D,* the temporal profile of U266 cells. The combined effects of ACHP and vincristine or PAM. U266 cells were cultured with vincristine or PAM (1-50 μmol/L) and combined with ACHP (10 μmol/L) for up to 5 days. Cell growth was assessed at day 1, day 3, and day 5. The growth of untreated control U266 cells at day 1, day 3, and day 5 was 175%, 448%, and 972%, respectively.

eventually resulted in the lack of response to the lymphotoxin β receptor signaling (36) and the failure of nuclear translocation of NF-κB (37). Owing to Ser536 being located within the carboxyl-terminal transactivation domain of p65, it is implicated in the transcriptional activity of NF-κB once bound to the target DNA within the regulatory region of target genes by recruiting basal transcription factors and transcriptional coactivators (20, 36, 38). In contrast, although the Ser529 phosphorylation was found associated with the signal-induced NF-κB activation through casein kinase II (39), it is unlikely that Ser529 plays a regulatory role in the NF-κB activation cascade and its phosphorylation is considered to occur as a coincidence (40). Regarding the Ser276 phosphorylation of p65, both protein kinase A and mitogen- and stress-activated protein kinase 1 have been implicated and are considered to be involved in the NF-κB activation by regulating the selective interaction with the p300/CREB-binding protein coactivator over histone deacetylase 1 (41, 42). However, other studies have shown that protein kinase A plays a negative role in the action of NF-κB (43, 44). Thus, Ser536 phosphorylation plays a major role in the signal-mediated regulation of transcriptional competence of NF-κB.

More importantly, the signal transduction pathways mediated by CD40L and B-cell activating factor have been shown to play important roles in the proliferation of myeloma cells. For example, B-cell activating factor is overexpressed in myeloma cells and involved in the protection from dexamethasone-induced apoptosis (45). In addition, CD40L is known to induce the proliferation and migration of myeloma cells by inducing NF-κB through the activation of mitogen-activated protein kinases and phosphatidylinositol-3 kinase (5). In another report, it is shown that CD40/CD40L signaling activates NF-κB by inducing the Ser536 phosphorylation of p65 (46). Although both IKKα and IKKβ have been implicated in the Ser536 phosphorylation (36, 37, 40), the signaling cascades involving CD40L, B-cell activating factor, and lymphotoxin β require IKKα but not IKKβ (36, 47, 48). Thus, IKKα could be a more feasible target for the treatment of multiple myeloma.

Furthermore, recent recognition of the noncanonical NF-κB activation cascade, which is used by the signaling mediated by B-cell activating factor, CD40L, and lymphotoxin β, and primarily involving IKKα but not necessarily associated with phosphorylation of IκBα proteins followed by their degradation, has highlighted the role of IKKα (49). Interestingly, the treatment of cells with a nuclear export inhibitor leptomycin B resulted in the nuclear accumulation of NF-κB, IκBα, NF-κB-inducing kinase, and IKKα, but not IKKβ, indicating that these proteins are shuttling between the cytoplasm and the nucleus even in the absence of any stimulation (50). Therefore, the sole inhibition of IKKβ or proteasome may not be sufficient to suppress the NF-κB activation associated with multiple myeloma.

In this study, ACHP exhibited the distinctive effective concentrations in inhibiting various features of myeloma cells. Although inhibition of the TNFα-mediated gene expression could occur at low ACHP concentration (<1 μmol/L), higher concentrations (>10 μmol/L) were required to inhibit the constitutive phosphorylation of p65, expression of NF-κB-mediated genes, such as *cyclin D1*, *bcl-x_L*, *XIAP*, *c-IAP1*, and *IL-6*, and myeloma cell growth. These findings indicate that the growth inhibitory effect of ACHP may be through the inhibition of IKKα as well as IKKβ.

In conclusion, our findings indicate the therapeutic efficacy ofACHP in inducing myeloma cell death presumably by blocking the constitutive activation of NF-κB and the induction of antiapoptotic genes, thus sensitizing myeloma cells to cell death mediated by conventional antimyeloma agents. Although further efforts in drug development are necessary (i.e., the search for IKKα-specific compounds), our findings obtained with ACHP should give useful insights into a novel antimyeloma chemotherapy. Use of such compounds would conceivably reduce the dose of antimyeloma agents, prevent the side effects, enhance the adherence to chemotherapy, and augment the efficacy of the current myeloma chemotherapy.

ACKNOWLEDGMENTS

We thank Angelita Sarile for the language editing of this manuscript.

REFERENCES

1. Hideshima T, Anderson KC. Molecular mechanisms of novel therapeutic approaches for multiple myeloma. Nat Rev Cancer 2002;2:927–37.

2. Iida S, Ueda R. Multistep tumorigenesis of multiple myeloma: its molecular delineation. Int J Hematol 2003;77:207–12.

3. Dankbar B, Padro T, Leo R, et al. Vascular endothelial growth factor and interleukin-6 in paracrine tumor-stromal cell interactions in multiple myeloma. Blood 2000;95:2630–6.

4. Pahl HL. Activators and target genes of Rel/NF-κB transcription factors. Oncogene 1999;18:6853–66.

5. Tai YT, Podar K, Mitsiades N, et al. CD40 induces human multiple myeloma cell migration via phosphatidylinositol 3-kinase/AKT/NF-κB signaling. Blood 2003;101:2762–9.

6. Mitsiades CS, Mitsiades N, Poulaki V, et al. Activation of NF-κB and up-regulation of intracellular antiapoptotic proteins via the IGF-1/Akt signaling in human multiple myeloma cells: therapeutic implications. Oncogene 2002;21:5673–83.

7. Hideshima T, Chauhan D, Schlossman R, Richardson P, Anderson KC. The role of tumor necrosis factor α in the pathophysiology of human multiple myeloma: therapeutic applications. Oncogene 2001;20:4519–27.

8. Mori N, Yamada Y, Ikeda S, et al. Bay 11-7082 inhibits transcription factor NF-κB and induces apoptosis of HTLV-I-infected T-cell lines and primary adult T-cell leukemia cells. Blood 2002;100: 1828–34.

9. Davis RE, Staudt LM. Molecular diagnosis of lymphoid malignancies by gene expression profiling. Curr Opin Hematol 2002;9:333–8.

10. Pikarsky E, Porat RM, Stein I, et al. NF-κB functions as a tumour promoter in inflammation-associated cancer. Nature 2004;431:461–6.

11. Greten FR, Eckmann L, Greten TF, et al. IKKβ links inflammation and tumorigenesis in a mouse model of colitis-associated cancer. Cell 2004;118:285–96.

12. Adams J. The proteasome: a suitable antineoplastic target. Nat Rev Cancer 2004;4:349–60.

13. Okamoto T, Sakurada S, Yang JP, Merin JP. Regulation of NF-κB and disease control: identification of a novel serine kinase and thioredoxin as effectors for signal transduction pathway for NF-κB activation. Curr Top Cell Regul 1997;35:149–61.

14. Nakano H, Shindo M, Sakon S, et al. Differential regulation of IκB kinase α and β by two upstream kinases, NF-κB-inducing kinase and mitogen-activated protein kinase/ERK kinase kinase-1. Proc Natl Acad Sci U S A 1998;95:3537–42.

15. Yang J, Lin Y, Guo Z, et al. The essential role of MEKK3 in TNF-induced NF-κB activation. Nat Immunol 2001;2:620–4.

16. DiDonato JA, Hayakawa M, Rothwarf DM, Zandi E, Karin M. A cytokine-responsive IκB kinase that activates the transcription factor NF-κB. Nature 1997;388:548–54.

17. Mercurio F, Zhu H, Murray BW, et al. IKK-1 and IKK-2: cytokine-activated IκB kinases essential for NF-κB activation. Science 1997;278:860–6.

18. Zandi E, Rothwarf DM, Delhase M, Hayakawa M, Karin M. The IκB kinase complex (IKK) contains two kinase subunits, IKKα and IKKβ, necessary for IκB phosphorylation and NF-κB activation. Cell 1997;91:243–52.

19. Sakurai H, Suzuki S, Kawasaki N, et al. Tumor necrosis factor-α–induced IKK phosphorylation of NF-κB p65 on serine 536 is mediated through the TRAF2, TRAF5, and TAK1 signaling pathway. J Biol Chem 2003;278:36916–23.

20. Jiang X, Takahashi N, Ando K, et al. NF-κB p65 transactivation domain is involved in the NF-κB-inducing kinase pathway. Biochem Biophys Res Commun 2003;301:583–90.

21. Murata T, Shimada M, Sakakibara S, et al. Discovery of novel and selective IKK-β serine-threonine protein kinase inhibitors: Part 1. Bioorg Med Chem Lett 2003;13:913–8.

22. Murata T, Shimada M, Sakakibara S, et al. Synthesis and structure-activity relationships of novel IKK-β inhibitors: Part 3. Orally active anti-inflammatory agents. Bioorg Med Chem Lett 2004;14:4019–22.

23. Kato M, Iida S, Komatsu H, Ueda R. Lack of ku80 alteration in multiple myeloma. Jpn J Cancer Res 2002;93:359–62.

24. Algarte M, Lecine P, Costello R, et al. *In vivo* regulation of interleukin-2 receptor α gene transcription by the coordinated binding of constitutive and inducible factors in human primary T cells. EMBO J 1995;14:5060–72.

25. Bharti AC, Donato N, Singh S, Aggarwal BB. Curcumin (diferuloylmethane) down-regulates the constitutive activation of nuclear factor-κB and IκBα kinase in human multiple myeloma cells, leading to suppression of proliferation and induction of apoptosis. Blood 2003;101:1053–62.

26. Yang JP, Hori M, Sanda T, Okamoto T. Identification of a novel inhibitor of nuclear factor-κB, RelA-associated inhibitor. J Biol Chem 1999;274:15662–70.

27. Sato T, Asamitsu K, Yang JP, et al. Inhibition of human immunodeficiency virus type 1 replication by a bioavailable serine/threonine kinase inhibitor, fasudil hydrochloride. AIDS Res Hum Retroviruses 1998;14:293–8.

28. Ando T, Kawabe T, Ohara H, et al. Involvement of the interaction between p21 and proliferating cell nuclear antigen for the maintenance of G_2/M arrest after DNA damage. J Biol Chem 2001;276:42971–7.

29. Kajino S, Suganuma M, Teranishi F, et al. Evidence that *de novo* protein synthesis is dispensable for antiapoptotic effects of NF-κB. Oncogene 2000;19:2233–9.

30. Specht K, Haralambieva E, Bink K, et al. Different mechanisms of cyclin D1 overexpression in multiple myeloma revealed by fluorescence *in situ* hybridization and quantitative analysis of mRNA levels. Blood 2004;104:1120-6.

31. Hideshima T, Bergsagel PL, Kuehl WM, Anderson KC. Advances in Biology of Multiple Myeloma: Clinical Applications. Blood 2004;104:603–18.

32. Hideshima T, Chauhan D, Richardson P, et al. NF-κB as a therapeutic target in multiple myeloma. J Biol Chem 2002;277:16639–47.

33. Dai Y, Pei XY, Rahmani M, et al. Interruption of the NF-κB pathway by Bay 11-7082 promotes UCN-01-mediated mitochondrial dysfunction and apoptosis in human multiple myeloma cells. Blood 2004;103:2761–70.

34. Mitsiades N, Mitsiades CS, Poulaki V, et al. Biologic sequelae of nuclear factor-κB blockade in multiple myeloma: therapeutic applications. Blood 2002;99:4079–86.

35. Bharti AC, Shishodia S, Reuben JM, et al. Nuclear factor-κB and STAT3 are constitutively active in CD138+ cells derived from multiple myeloma patients, and suppression of these transcription factors leads to apoptosis. Blood 2004;103:3175–84.

36. Jiang X, Takahashi N, Matsui N, Tetsuka T, Okamoto T. The NF-κB activation in lymphotoxin β receptor signaling depends on the phosphorylation of p65 at serine 536. J Biol Chem 2003;278:919–26.

37. Mattioli I, Sebald A, Bucher C, et al. Transient and selective NF-κB p65 serine 536 phosphorylation induced by T cell costimulation is mediated by IκB kinase β and controls the kinetics of p65 Nuclear Import. J Immunol 2004;172:6336–44.

38. Asamitsu K, Tetsuka T, Kanazawa S, Okamoto T. RING finger protein AO7 supports NF-κB-mediated transcription by interacting with the transactivation domain of the p65 subunit. J Biol Chem 2003;278:26879–87.

39. Wang D, Westerheide SD, Hanson JL, Baldwin AS Jr. Tumor necrosis factor α–induced phosphorylation of RelA/p65 on Ser529 is controlled by casein kinase II. J Biol Chem 2000;275:32592–7.

40. Sakurai H, Chiba H, Miyoshi H, Sugita T, Toriumi W. IκB kinases phosphorylate NF-κB p65 subunit on serine 536 in the transactivation domain. J Biol Chem 1999;274:30353–6.

41. Zhong H, May MJ, Jimi E, Ghosh S. The phosphorylation status of nuclear NF-κB determines its association with CBP/p300 or HDAC-1. Mol Cell 2002;9:625–36.

42. Vermeulen L, De Wilde G, Van Damme P, Vanden Berghe W, Haegeman G. Transcriptional activation of the NF-κB p65 subunit by mitogen- and stress-activated protein kinase-1 (MSK1). EMBO J 2003;22:1313–24.

43. Takahashi N, Tetsuka T, Uranishi H, Okamoto T. Inhibition of the NF-κB transcriptional activity by protein kinase A. Eur J Biochem 2002;269:4559–65.

44. Neumann M, Grieshammer T, Chuvpilo S, et al. RelA/p65 is a molecular target for the immunosuppressive action of protein kinase A. EMBO J 1995;14:1991–2004.

45. Moreaux J, Legouffe E, Jourdan E, et al. BAFF and APRIL protect myeloma cells from apoptosis induced by interleukin 6 deprivation and dexamethasone. Blood 2004;103:3148–57.

46. Schwabe RF, Schnabl B, Kweon YO, Brenner DA. CD40 activates NF-κB and c-Jun N-terminal kinase and enhances chemokine secretion on activated human hepatic stellate cells. J Immunol 2001;166:6812–9.

47. Coope HJ, Atkinson PG, Huhse B, et al. CD40 regulates the processing of NF-κB2 p100 to p52. EMBO J 2002;21:5375–85.

48. Claudio E, Brown K, Park S, Wang H, Siebenlist U. BAFF-induced NEMO-independent processing of NF-κB2 in maturing B cells. Nat Immunol 2002;3:958–65.

49. Pomerantz JL, Baltimore D. Two pathways to NF-κB. Mol Cell 2002;10:693–5.

50. Birbach A, Gold P, Binder BR, et al. Signaling molecules of the NF-κB pathway shuttle constitutively between cytoplasm and nucleus. J Biol Chem 2002;277:10842–51.

53BP2 induces apoptosis through the mitochondrial death pathway

Shinya Kobayashi[1,2,†], Shinichi Kajino[1,2,†], Naoko Takahashi[1], Satoshi Kanazawa[1], Kenichi Imai[1], Yurina Hibi[1], Hirotaka Ohara[2], Makoto Itoh[2] and Takashi Okamoto[1,*]

[1]Department of Molecular and Cellular Biology, and [2]Department of Internal Medicine and Bioregulation, Nagoya City University Graduate School of Medical Sciences, 1 Kawasumi, Mizuho-cho, Mizuho-ku, Nagoya, Aichi 467-8601, Japan

The p53 binding protein 2 (53BP2) has been identified as the interacting protein to p53, Bcl-2, and p65 subunit of nuclear factor κB (NF-κB). The TP53BP2 gene encodes two splicing variants, 53BP2S and 53BP2L, previously known as apoptosis stimulating protein 2 of p53 (ASPP2). We found that these 53BP2 proteins are located predominantly in the cytoplasm and induce apoptosis as demonstrated by cleavage of poly ADP ribose polymerase (PARP) and annexin V staining. Furthermore, we demonstrate that 53BP2 is located in the mitochondria and induces apoptosis associated with depression of the mitochondrial trans-membrane potential ($\Delta\Psi m$) and activation of caspase-9. From these findings we conclude that 53BP2 induces apoptosis through the mitochondrial death pathway.

Introduction

Apoptosis is a well-defined biochemical pathway and is essential for the maintenance of cellular homeostasis in metazoans. Accumulating evidences indicate that the normal apoptotic pathway is affected in the pathological processes such as cancer and autoimmunity (Fisher *et al.* 1995; Green & Reed 1998; Jackson & Puck 1999; Daniel & Korsmeyer 2004). The induction of apoptosis occurs through two distinct pathways, the one elicited by death receptors in the plasma membrane ('extrinsic pathway') and the other directly involving mitochondria ('intrinsic pathway'). Whereas the former primarily involves activation of caspase-8, the latter apoptosis pathway is associated with the release of cytochrome C from mitochondria and activation of caspase-9 (for a review see Judith *et al.* 2004).

The p53 binding protein 2 (53BP2) has been initially identified as an interacting protein to p53 (Iwabuchi *et al.* 1994) and implicated in the biological action of p53. It was also shown that the 53BP2 binding site in the p53 core domain is evolutionarily conserved and is frequently mutated in human cancer (Iwabuchi *et al.* 1994; Gorina & Pavletich 1996). The subsequent studies have revealed that it interacts with Bcl-2 (Naumovski & Cleary 1996) and p65 subunit of nuclear factor κB (NF-κB) (Yang *et al.* 1999). Interestingly, 53BP2 has been shown to induce apoptosis (Yang *et al.* 1999), which was confirmed by others (Lopez *et al.* 2000; Ao *et al.* 2001; Samuels-Lev *et al.* 2001; Bergamaschi *et al.* 2004). However, the mechanism by which 53BP2 induces apoptosis has not been clarified.

53BP2 protein is encoded by a single copy gene *TP53BP2* located in the long arm of chromosome 1 at q42.1 (Yang *et al.* 1997). We have recently found that it encodes two distinct mRNA species, either with or without exon 3, by alternative splicing (Takahashi *et al.* 2004) (Fig. 1A). These splicing variants encode two 53BP2 proteins containing 1005 and 1128 amino acids (aa) with the longer isoform containing additional 123 amino acids in the N-terminus where no known functional motif or distinct intracellular localization signal is found. Although Samuels-Lev *et al.* (2001) renamed the longer 53BP2 isoform as ASPP2 (apoptosis stimulating protein of p53 2), we have proposed to call these proteins as 53BP2S (short) and 53BP2L (long) based on the genome organization of *TP53BP2* transcripts (Takahashi *et al.* 2004). 53BP2 proteins contain several structural and functional motifs including Gln-rich α-helical region, Pro-rich regions, ankyrin repeats, and Src-homology 3 domain.

Communicated by: Masayuki M. Yamamoto
**Correspondence*: E-mail: tokamoto@med.nagoya-cu.ac.jp
†These two authors contributed equally to this work.

DOI: 10.1111/j.1365-2443.2005.00835.x

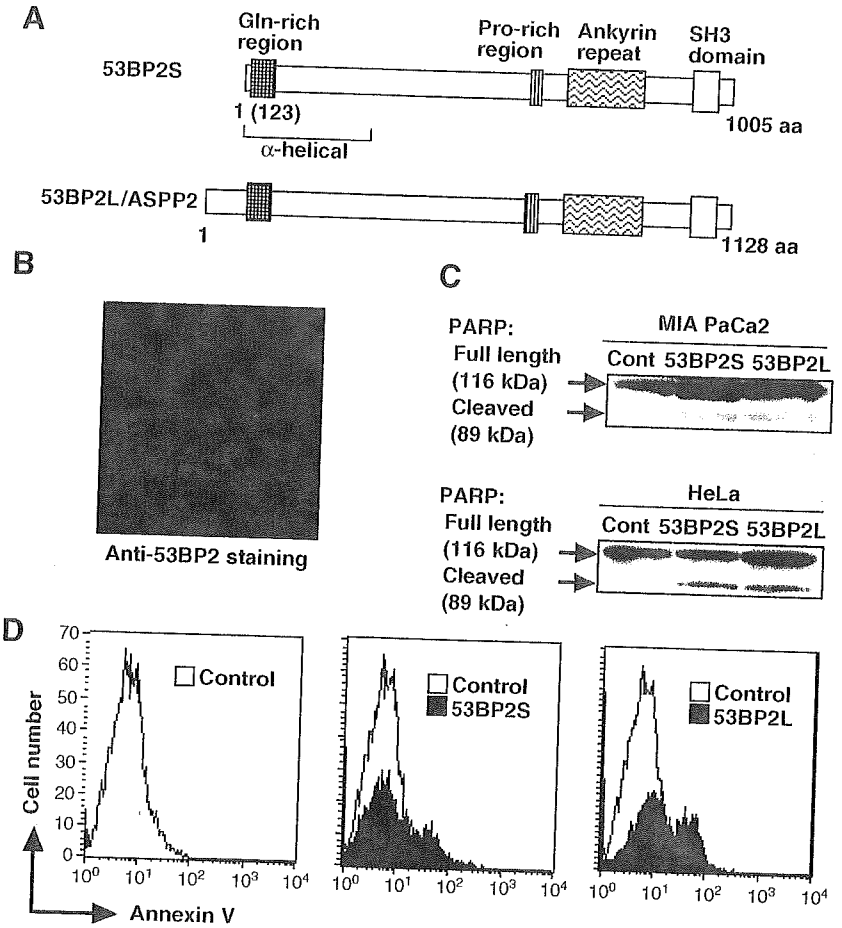

Figure 1 Induction of apoptosis by 53BP2 proteins. (A) Diagrammatic representation of 53BP2S and 53BP2L/ASPP2 proteins. Locations of Gln-rich region, putative 'α-helical region,' Pro-rich region, ankyrin repeats, and SH3 domain are indicated. Two splicing variants, 53BP2S and 53BP2L/ASPP2, containing 1005 amino acids and 1128 amino acids residues, respectively, are encoded by the same gene *TP53BP2* (Takahashi *et al.* 2004). 53BP2L contains additional 123 amino acid N-terminal region containing no apparent functional/structural motifs. (B) The localization of endogenous 53BP2 proteins in MIA PaCa-2 cells. Subcellular localization of endogenous 53BP2 was examined by immunostaining with anti-53BP2 mouse monoclonal antibody. The dim staining of 53BP2 proteins was repeatedly observed, which is presumably due to the low protein stability as previously indicated (Yang *et al.* 1999; Lopez *et al.* 2000). (C) Cleavage of PARP by 53BP2 proteins. MIA PaCa-2 cells and HeLa cells were transfected with pcDNA3.1–53BP2 ('53BP2S') or pCEP4-ASPP2 ('53BP2L') plasmids and the cell lysates were immunoblotted with anti-PARP antibody. The intact form of PARP (116 kDa) and its cleavage form (89 kDa) were detected by an anti-PARP rabbit polyclonal antibody (indicated by arrows). Note that no significant difference of the amounts of the cleaved form of PARP was found in cells expressing 53BP2S and 53BP2L. Cont, cells transfected with a control expression vector pcDNA3.1. (D) Induction of apoptosis by over-expression of 53BP2 proteins. MIA PaCa-2 cells were transfected with pcDNA3.1–53BP2 or pCEP4-ASPP2 and cells undergoing apoptosis were detected by flow cytometry. Live and dead cells were discriminated on the basis of their forward and side light-scattering properties. In order to evaluate cells undergoing apoptosis, cells were stained by both annexin V-PE and 7-AAD and those cells expressing 7-AAD were excluded from the measurement. The transfection efficiency was estimated to be approximately 65% by the GFP expression from the co-transfected pEGFP plasmid. The experiments were repeated more than three times with the same results.

In this study, we demonstrate that two 53BP2 isoforms, 53BP2S (previously called '53BP2') and 53BP2L ('ASPP2'), are localized predominantly in the cytoplasm and similarly induce apoptosis. We found that the mitochondrial death pathway is involved in the 53BP2-mediated apoptosis. The biological roles of 53BP2 and its interacting proteins in the regulation of apoptosis are discussed.

Results

Induction of apoptosis by 53BP2 proteins

Figure 1A illustrates the organization of 53BP2 isoforms as previously reported (Takahashi *et al.* 2004). As shown in Fig. 1B, the endogenous 53BP2 proteins were localized predominantly in the cytoplasm, confirming the previous reports wherein 53BP2 was over-expressed (Iwabuchi *et al.* 1998; Yang *et al.* 1999). To compare the effect of 53BP2S and 53BP2L, these proteins were transduced in MIA PaCa-2 and HeLa cells. After 48 h of transfection, the cleaved form of poly ADP ribose polymerase (PARP; 89 kDa product), a hallmark of apoptosis, was detected (Fig. 1C). When 53BP2S and 53BP2L were over-expressed in MIA PaCa-2 cells, approximately 16% and 27% of cells were found undergoing early apoptotic process (annexin V (+), 7-AAD (–)), respectively, whereas the percentage of apoptotic cells in the control was only 1.8% (Fig. 1D). The extents of apoptosis were similar to our previous observations using various DNA damaging agents (Mori *et al.* 2000).

Induction of apoptosis in a stable transfectant (293/53BP2)

We then examined the action of 53BP2 using the 293/53BP2 cells, in which expression of 53BP2S is under stringent control by ponasteron A (pon A). In Fig. 2A, both 293/53BP2 and its control 293/LZ were treated with pon A. The 53BP2S protein became detectable after 12 h of induction by pon A (5 μM) in a time-dependent manner and induced apoptosis as early as 24 h after pon A treatment. As shown in Fig. 2B, after 72 h of 53BP2S expression, a significant number (26%) of cells underwent apoptosis as revealed by positive staining for annexin V, whereas only the background level (6.5%) was stained in control cells. Cells at early apoptotic process (annexin (+), 7-AAD (–)) were found 14% and 3% in 293/53BP2 cells and control cells, respectively (Fig. 2B). No cleavage of PARP or a significant annexin V staining was detected with the control 293/LZ cells (data not shown).

Cytosolic and mitochondrial localization of 53BP2S

In Fig. 3A, intracellular localization of 53BP2S was examined by transfection of pEGFP53BP2 expressing 53BP2S in fusion with green fluorescence protein (GFP). A punctate vesicular pattern was noted, localized predominantly in the cytoplasm of the transfected cells. To confirm the localization of 53BP2S, we co-transfected pDsRed2-Mito, expressing red fluorescent protein targeted to mitochondria. As demonstrated in Fig. 3A and

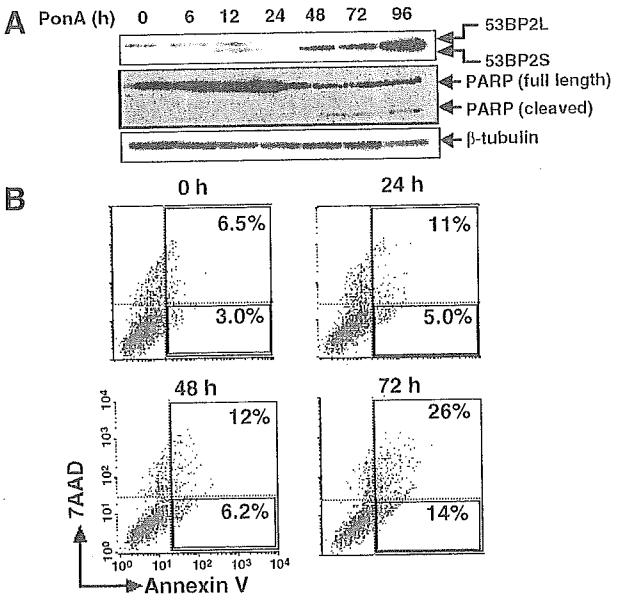

Figure 2 Induction of apoptosis in 293/53BP2 cell line. (A) Time course of induction of 53BP2S and cleavage of PARP in 293/53BP2 cells. Cells were treated with pon A (5 μM) using an ecdysone-inducible expression system for the indicated periods (h), and the cell lysate (10 μg protein) was examined for the expression of 53BP2S and PARP. The intact full-length PARP (116 kDa) was cleaved into 89 kDa during the apoptotic process. Longer exposure of chemiluminescence for protein detection revealed the endogenous 53BP2L protein in these cells. β-tubulin was used as an internal control. (B) Flow cytometric detection of apoptotic cells. 293/53BP2 cells were stimulated with pon A (5 μM) and cultured for the indicated periods (h). The percentages of cells at apoptosis (annexin V (+)) and cells at early apoptosis (annexin V positive and 7-AAD (–)) were counted and indicated separately.

53BP2S was shown to be partly localized in the mitochondria in addition to the cytoplasm. In most cells only portions of mitochondria were costained with 53BP2S, suggesting that small amounts of 53BP2S molecules could be sufficient to induce apoptosis. In Fig. 3B, subcellular fractionation was performed and the presence of 53BP2S was examined. Protein expression was induced by pon A for 48 h and each subcellular fraction was subjected to Western blotting with anti-53BP2 antibody. Although majority of the 53BP2S protein was detected in the cytosolic fraction, it was also detected in the mitochondrial fraction (Fig. 3B).

Depression of $\Delta\Psi$m by 53BP2S expression

These findings suggested the involvement of the 'intrinsic' death pathway. We thus examined the change in $\Delta\Psi$m

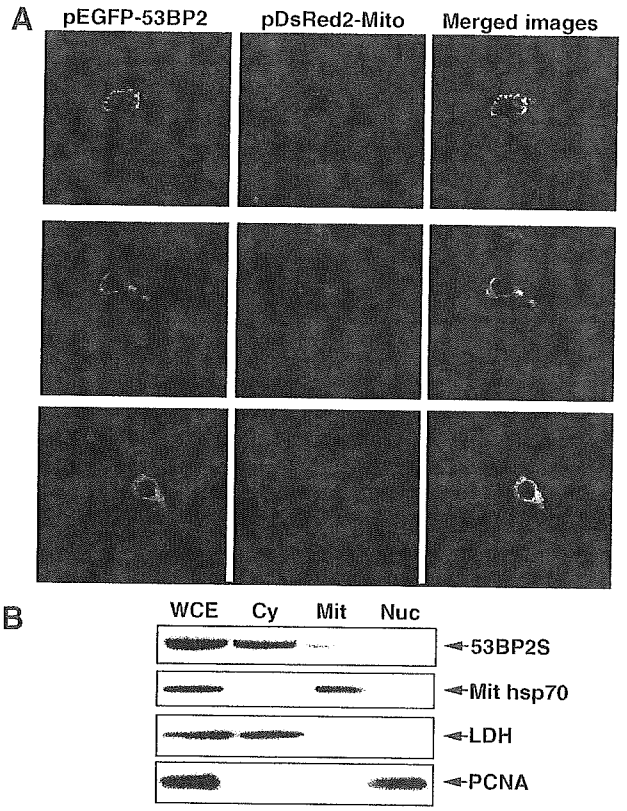

Figure 3 Intracellular localization of 53BP2S. (A) Co-localization of 53BPS and mitochondria marker. 293 cells were transiently transfected with pEGFP-53BP2 and mitochondria-targeting plasmid pDsRed2-Mit and examined under confocal microscope. The GFP fluorescence, DsRed fluorescence and merged images of cells are shown. Note that only portions of mitochondria (visualized by DsRed) were costained with GFP (53BP2S). (B) Subcellular fractionation. Upon induction of 53BP2 by pon A (5 μM, 48 h) in 293/53BP2 cells, whole cell extract (WCE) was prepared. The cytoplasmic (Cy), mitochondrial (Mit) and nuclear (Nuc) fractions were separated as described in Experimental procedures. Each protein fraction was separated by 10% SDS-PAGE, and probed with antibodies to 53BP2S, PCNA (nuclear marker), mitochondrial heat shock protein (Mit hsp70) and LDH (cytoplasmic marker). The same cell equivalents were loaded on each lane. Contamination of the cytoplasmic fraction into the mitochondria fraction was considered negligible because of the absence of LDH. The identical results were obtained repeatedly.

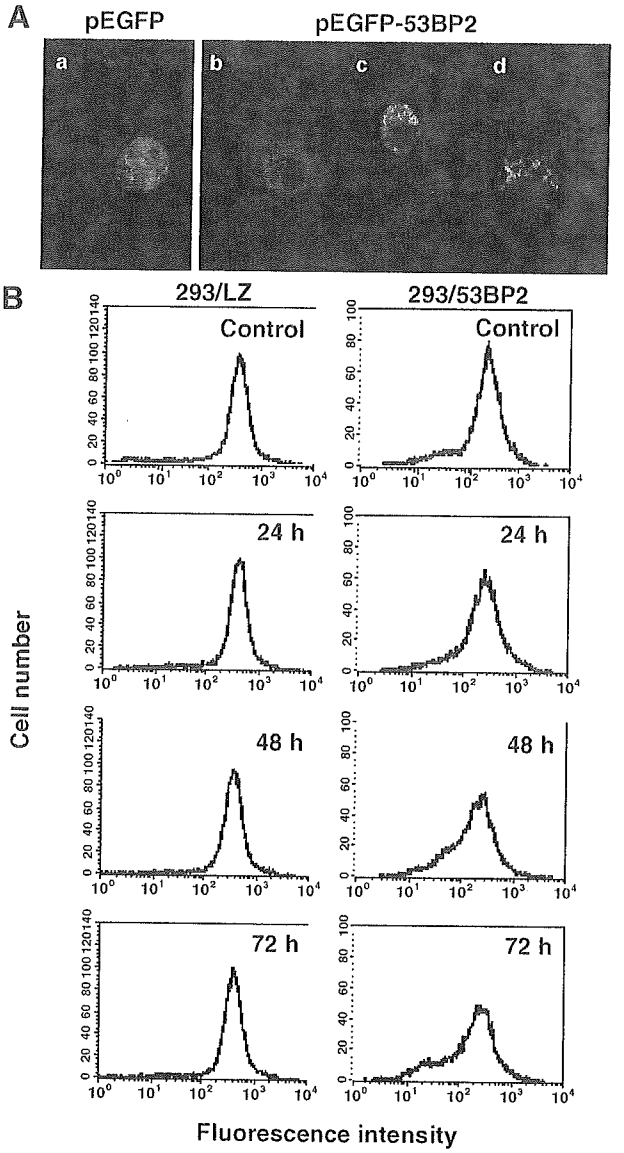

Figure 4 Alteration of the mitochondria transmembrane potential ($\Delta\Psi m$) by 53BP2S. (A) Reduction of $\Delta\Psi m$ by 53BP2S. After 48 h of transfection with pEGFP (a) or pEGFP53BP2 (b–d) plasmids, MIA PaCa-2 cells were stained with CMXRos. Typical cells are shown. In cells expressing 53BP2S, progressive reduction of $\Delta\Psi m$ was observed in association with nuclear fragmentation (from b–d). The same exposure time was used in each picture. (B) Temporal change of $\Delta\Psi m$ following 53BP2S induction. 293/53BP2 and 293/LZ cells were treated with pon A for indicated periods (h), stained with rhodamine 123, and flow cytometric analysis was performed. Distribution of fluorescence intensity of cells with sham treatment (only the solvent ethanol was added) is shown in gray shadow. 'Control,' uninduced cells.

following 53BP2S expression (Fig. 4). Several cationic, lipophilic, fluorescent dyes such as CMXRos and rhodamine 123, can readily detect changes in $\Delta\Psi m$ as they are selectively sequestered by respiring mitochondria by virtue of their negative charges on the inner membrane and are washed out when $\Delta\Psi m$ is lost. As shown in Fig. 4A, the extent of CMXRos staining in pEGFP53BP2-transfected cells (visualized by the expression of GFP)